Targeted imaging of matrix metalloproteinase activity in the evaluation of remodeling tissue-engineered vascular grafts implanted in a growing lamb model

Mitchel R. Stacy, PhD,[a] Yuji Naito, MD, PhD,[b] Mark W. Maxfield, MD,[a] Hirotsugu Kurobe, MD, PhD,[c] Shuhei Tara, MD, PhD,[c] Chung Chan, PhD,[a] Kevin A. Rocco, MS,[a] Toshiharu Shinoka, MD, PhD,[c] Albert J. Sinusas, MD,[a] and Christopher K. Breuer, MD[c]

Objectives: The clinical translation of tissue-engineered vascular grafts has been demonstrated in children. The remodeling of biodegradable, cell-seeded scaffolds to functional neovessels has been partially attributed to matrix metalloproteinases. Noninvasive assessment of matrix metalloproteinase activity can indicate graft remodeling and elucidate the progression of neovessel formation. Therefore, matrix metalloproteinase activity was evaluated in grafts implanted in lambs using in vivo and ex vivo hybrid imaging. Graft growth and remodeling was quantified using in vivo x-ray computed tomography angiography.

Methods: Cell-seeded and unseeded scaffolds were implanted in 5 lambs as inferior vena cava interposition grafts. At 2 and 6 months after implantation, in vivo angiography was used to assess graft morphology. In vivo and ex vivo single photon emission tomography/computed tomography imaging was performed with a radiolabeled compound targeting matrix metalloproteinase activity at 6 months. The neotissue was examined at 6 months using qualitative histologic and immunohistochemical staining and quantitative biochemical analysis.

Results: The seeded grafts demonstrated significant luminal and longitudinal growth from 2 to 6 months. In vivo imaging revealed subjectively greater matrix metalloproteinase activity in grafts versus native tissue. Ex vivo imaging confirmed a quantitative increase in matrix metalloproteinase activity and demonstrated greater activity in unseeded versus seeded grafts. The glycosaminoglycan content was increased in seeded grafts versus unseeded grafts, without significant differences in collagen content.

Conclusions: Matrix metalloproteinase activity remained elevated in tissue-engineered grafts 6 months after implantation and could indicate remodeling. Optimization of in vivo imaging to noninvasively evaluate matrix metalloproteinase activity could assist in the serial assessment of vascular graft remodeling. (J Thorac Cardiovasc Surg 2014;148:2227-33)

See related commentary on page 2234.

Our research team developed the first tissue-engineered vascular graft (TEVG) to be used in humans[1] and applied this technology in a clinical trial for congenital heart surgery.[2] We are currently conducting the first Food and Drug Administration–approved clinical trial examining the safety and efficacy of TEVG implantation in children within the United States.[3] The TEVGs were constructed with autologous bone marrow mononuclear cells (BM-MNCs) seeded onto a biodegradable scaffold[4] and demonstrated growth potential in vivo,[5] making the grafts ideally suited for application in infants and children.

The transition of a cell-seeded scaffold to a neovessel is a process characterized by scaffold degradation as a result of hydrolysis, cellular infiltration, and extracellular matrix (ECM) deposition and remodeling.[6] Matrix metalloproteinases (MMPs) are enzymes thought to play important roles in tissue homeostasis and functional growth and might contribute significantly to ECM remodeling during neovessel formation.[6,7] Specifically, MMP-2 and -9 are basement membrane-degrading MMPs that can play critical roles in ECM remodeling. Previous postmortem examinations of TEVGs implanted in a murine model have demonstrated progressively greater MMP-2 expression during a 4-week course after TEVG implantation,

From the Yale University School of Medicine,[a] New Haven, Conn; University of California, San Francisco,[b] Benioff Children's Hospital, San Francisco, Calif; and Nationwide Children's Hospital,[c] Columbus, Ohio.

The present study was supported in part by National Institutes of Health grant T32 HL098069 (to A.J.S.) and the Charles W. Ohse Research Award (Department of Surgery, Yale University School of Medicine; to M.W.M.).

Disclosures: Drs Breuer and Shinoka received financial support from the Gunze Corporation. The RP805 compound was supplied to Dr Sinusas from Lantheus Medical Imaging, Inc. All other authors have nothing to disclose with regard to commercial support.

Drs Stacy and Naito contributed equally to this work.

Received for publication Dec 19, 2013; revisions received April 23, 2014; accepted for publication May 16, 2014; available ahead of print June 18, 2014.

Address for reprints: Christopher K. Breuer, MD, Nationwide Children's Hospital, 700 Children's Dr, Columbus, OH 43205 (E-mail: christopher.breuer@nationwidechildrens.org).

0022-5223/$36.00

http://dx.doi.org/10.1016/j.jtcvs.2014.05.037

Abbreviations and Acronyms

BM-MNC = bone marrow mononuclear cell
CT = computed tomography
ECM = extracellular matrix
IVC = inferior vena cava
MMP = matrix metalloproteinase
SPECT = single photon emission CT
^{99m}Tc = technetium-99m
TEVG = tissue engineered vascular graft

and MMP-9 expression peaked at 1 week after surgery and had significantly decreased by 4 weeks.[6] The elevated MMP-2 expression within a murine model of TEVG is consistent with the postmortem findings of Cummings and colleagues,[7] who observed elevated MMP-2 expression in a lamb model of TEVG implantation; however, MMP-9 expression also remained elevated for 80 weeks after implantation. These results suggest that MMPs could play a role in the remodeling of TEVGs and that this process could be prolonged for many months after implantation.

The current clinical imaging techniques for the serial assessment of TEVG remodeling have focused on evaluation of the morphologic changes using x-ray computed tomography (CT) and magnetic resonance angiography[2,5]; however, these approaches cannot provide information related to the underlying mechanisms responsible for the ongoing neovessel formation. Targeted imaging of MMP activity has been previously demonstrated in animal models of atherosclerosis,[8-12] vascular remodeling,[13,14] and myocardial infarction[15,16] using single photon emission CT (SPECT) and magnetic resonance approaches. Additionally, near-infrared fluorescence imaging has indicated progressive remodeling in a murine model of TEVG implantation that was associated with qualitative elevations in MMP-2 and -9 activity.[17] The technetium-99m (^{99m}Tc)-labeled tracer, ^{99m}Tc-RP805, is a broad-spectrum MMP-targeted compound used for SPECT/CT imaging that can localize to the site of ECM remodeling and provide an opportunity to serially assess the progression of TEVG remodeling and the formation of functional neotissue. Therefore, we hypothesized that ^{99m}Tc-RP805 SPECT/CT imaging of MMP activity could complement standard noninvasive imaging approaches and might serve as a useful tool for serial assessment of neovessel formation. To test this hypothesis, we evaluated the feasibility of in vivo and ex vivo SPECT/CT imaging of MMP activity within TEVGs in a clinically relevant large animal model 6 months after TEVG implantation. We also evaluated the serial changes in TEVG morphology using CT angiography.

METHODS

Graft Scaffold

Scaffolds were constructed using a polyglycolic acid nonwoven sheet coated with a 50:50 copolymer solution of poly (L-lactic acid-co-ε-caprolactone; Gunze Corp, Tokyo, Japan), as previously described.[2] Before seeding, all grafts had a measured luminal diameter of 12 mm, wall thickness of 1.5 mm, and length of 20 mm (Figure 1, *A*). Graft porosity was examined using scanning electron microscopy (model XL-30; FEI Co, Hillsboro, Ore).

Bone Marrow-Derived Cell Isolation

Autologous BM-MNCs were isolated from the iliac crest or femoral head of 3 juvenile Dover lambs into a heparinized syringe (100 U/mL), diluted 1:4 in phosphate-buffered saline, and passed through a 100-μm filter to remove the fat and bone fragments. The bone marrow–phosphate-buffered saline solution was added to Histopaque-1077 (Sigma-Aldrich, St Louis, Mo) for density centrifugation at 1500 rpm for 30 minutes. The BM-MNCs were isolated and subsequently washed with phosphate-buffered saline and centrifuged (1500 rpm for 10 min) 2 more times. This cell isolation procedure was performed for each of the 3 lambs that were implanted with the cell-seeded scaffolds.

Scaffold Seeding

The scaffolds were added to a sterile vacuum seeding setup, as previously described.[18] Pressure of 50 mm Hg was applied to the system, thereby vacuum seeding the BM-MNCs onto the scaffolds. After seeding, the scaffolds were placed in autologous serum and incubated for 24 hours (37°C, 5% carbon dioxide, 95% relative humidity, 760 mm Hg). A sample of each graft was stained with Lee's methylene blue on glycol methacrylate-fixed tissue to quantify the number of attached cells.

Graft Implantation

TEVGs were implanted as inferior vena cava (IVC) interposition grafts (3 seeded scaffolds; 2 unseeded scaffolds) in 5 juvenile Dover lambs (implantation weight, 22.4 ± 2.3 kg). The lambs were sedated with intramuscular acepromazine (0.05 mg/kg), followed by intravenous diazepam (0.2 mg/kg) and ketamine (2.75 mg/kg). Anesthesia was maintained throughout surgery with 1% to 5% isoflurane and intravenous propofol (25 μg/kg/min). Perioperative cefazolin (22 mg/kg) was administered. A right thoracotomy was performed through the seventh intercostal space. After isolation of the IVC and dissection of the phrenic nerve, heparin (100 IU/kg) was administered intravenously. The IVC was then clamped for 5 minutes and unclamped for 2 minutes; this process was repeated 3 times for adequate conditioning. Next, a 2-cm TEVG was anastomosed (proximally and then distally) using running monofilament 5-0 suture. Radiopaque markers were placed at the anastomoses (Figure 1, *E*). Fibrin sealant (Tisseel; Baxter International, Deerfield, Ill) was used for hemostasis. A bupivacaine (Marcaine; Hospira, Lake Forest, Ill) nerve block was given for intercostal nerves 5 to 9. Layered closure was performed, and the chest tube was removed in the operating room. Postoperatively, the lambs were treated with fentanyl patches and flunixin meglumine (Banamine; Merck Animal Health, Whitehouse Station, NJ) for analgesia. No postoperative antiplatelets or anticoagulants were given. The Institutional Animal Care and Use Committee at Yale University approved the use of the lambs and all procedures. All the lambs received humane care in compliance with the "Guide for the Care and Use of Laboratory Animals" published by the National Institutes of Health, Animal Welfare Act, and Animal Welfare Regulations.

CT Angiography Imaging and Analysis

In vivo, 64-slice, x-ray CT angiography with iodinated contrast (350 mgI/mL; Omnipaque; GE Healthcare, Little Chalfont, UK) was performed

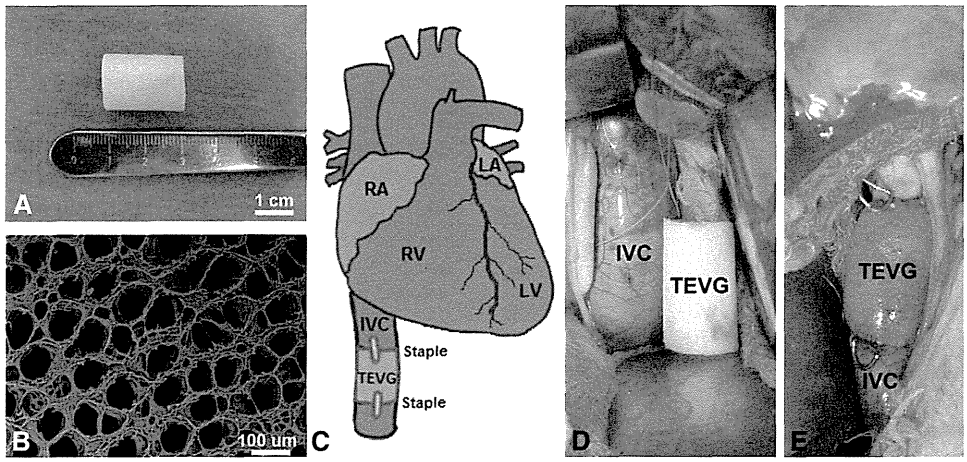

FIGURE 1. A, Graft scaffold and (B) scanning electron micrograph of polymer scaffold before surgical implantation. C, Schematic representation of surgical implantation of inferior vena cava interposition graft. Intraoperative photograph (D) before and (E) immediately after surgical implantation of an unseeded scaffold. Staples denote proximal and distal anastomoses. *RA*, Right atrium; *RV*, right ventricle; *LV*, left ventricle; *IVC*, inferior vena cava; *TEVG*, tissue engineered vascular graft; *LA*, left atrium.

(Discovery NM-CT 570c, GE Healthcare) in the lambs at 2 and 6 months after TEVG implantation to assess the graft luminal and longitudinal growth. After sedation, the lambs were intubated and mechanically ventilated (Venturi, Cardiopulmonary Corp, Milford, Conn) with 35% oxygen, 65% nitrous oxide, and 1% to 3% isoflurane. Blood pressure, oxygen saturation, and electrocardiographic signal were continuously monitored during each imaging session (IntelliVue MP50; Philips Healthcare, Best, The Netherlands). Peripheral vein access was established, and a 5F polyethylene catheter was placed for administration of fluids, CT contrast agent, and radioisotope. Before imaging, all the lambs were fasted overnight and given an intravenous 500-mL bolus of normal saline to attain euvolemia. CT images were acquired at a slice thickness of 0.625 mm at 300 mA and 120 kVp. Intravenous contrast injections were performed with a power injector (Stellant D; Medrad, Warrendale, Pa) at a constant rate of 3 mL/s and total volume of 30 mL, followed by a 20-mL saline flush at 3 mL/s. The TEVG luminal volume and length were quantified using commercially available software (Advanced Workstation, version 4.4; GE Healthcare). Measurement of the TEVG length was standardized by selecting the midpoint of each marker attached to the distal and proximal anastomoses. Stenosis was defined as a decrease in the luminal diameter that was >50% of the initial diameter at implantation.

In Vivo Hybrid SPECT/CT Imaging

In vivo single isotope imaging was performed 6 months after IVC graft implantation for qualitative assessment of MMP activity using hybrid SPECT/CT with ^{99m}Tc-RP805 (Lantheus Medical Imaging, Inc, North Billerica, Mass). ^{99m}Tc-RP805 is a broad-spectrum MMP-targeted compound that binds to the activated exposed catalytic domain of MMP-2, -3, -7, -9, -12, and -13. Previous work in our laboratory has demonstrated the various binding characteristics associated with this radiotracer for each of these MMPs.[16] SPECT was performed 60 minutes after intravenous injection of the radiotracer at rest (1468.9 ± 159.1 MBq). All images were acquired using a dedicated cardiac SPECT camera (Discovery 570c; GE Healthcare) at a 4-mm slice thickness. Immediately after each SPECT acquisition, noncontrast-enhanced CT images were acquired and reconstructed using filtered back projection to create CT attenuation maps. The SPECT images were reconstructed with a maximum a posteriori algorithm at 80 iterations using commercially available software (Xeleris; GE Healthcare). Smoothing parameters were selected as $\beta = 0.2$ and $\alpha = 0.41$. The images were reconstructed with a dimension of 150 × 150 × 150 voxels to alleviate artifacts that can result from truncated projections from the limited field-of-view associated with this SPECT system.[19] The attenuation map was incorporated into the reconstruction for attenuation correction. No postfiltering was applied to preserve the image resolution.

Ex Vivo SPECT/CT and Quantification

Ex vivo ^{99m}Tc-RP805 SPECT/CT was performed immediately after graft explantation. The grafts were placed on a conical tube to allow for circumferential visualization and differentiation of MMP activity in the graft wall. Immediately after each SPECT acquisition, noncontrast-enhanced CT images were acquired, as previously described. The SPECT images were reconstructed at a 2-mm slice thickness using the same reconstruction configuration as specified previously. The total counts were recorded on axial slices of the explanted graft and adjacent native IVC using the vendor's software (Xeleris; GE Healthcare) and normalized to the cross-sectional area of tissue for each axial slice. Retention of ^{99m}Tc-RP805 within the graft tissue and native IVC was expressed as a ratio (TEVG/native IVC).

Histologic Assessment

After surgical explantation and imaging, portions of the TEVG tissue and native IVC were fixed in 10% formalin and embedded in paraffin. Next, 5-μm sections, sampled from the midsection of the TEVG, were stained using standardized techniques for hematoxylin and eosin, Masson's trichrome (collagen), Alcian blue (glycosaminoglycans), and elastica van Gieson (elastin).

Biochemical Assessment

The collagen content was determined for the TEVG and native IVC tissue in triplicate using a Sircol soluble collagen assay (Biocolor Ltd, Carrickfergus, United Kingdom) according to the manufacturer's instructions. The glycosaminoglycan content was determined in triplicate using a Blyscan colorimetric assay (Biocolor Ltd) in a similar fashion.

Statistical Analysis

Statistical analysis was performed using commercially available software (GraphPad Prism, version 6.00, for Mac OS X; GraphPad Software, La Jolla, Calif). Paired *t* tests were used to evaluate the serial changes in luminal volume and graft length (determined from CT angiography) in

the seeded grafts. Unpaired *t* tests were used to evaluate the differences in the CT angiography, ex vivo ^{99m}Tc-RP805 SPECT/CT, and biochemical results between the seeded and unseeded grafts. Data are expressed as the mean ± standard deviation, unless stated otherwise. A biostatistician at the Research Institute, Nationwide Children's Hospital (Columbus, Ohio) reviewed all statistical analyses for proper methodology and interpretation.

RESULTS

Graft Scaffold and Cell Seeding

The scaffold matrix was approximately 80% porous, with pore diameters ranging from 20 to 100 μm (Figure 1, *B*). Isolation and seeding of the BM-MNCs onto the graft scaffolds (n = 3) resulted in the attachment of 3189 ± 2337 cells/mm^2 before surgical implantation. All 5 lambs survived the duration of the 6-month study without any graft-related complications.

CT Angiography

In vivo CT angiography demonstrated graft patency in all the lambs at 2 and 6 months after implantation (Figure 2). The seeded grafts had a significantly greater luminal volume at 6 months than at 2 months after implantation (2 months, 2.9 ± 0.9 cm^3; 6 months, 3.7 ± 0.9 cm^3; $P < .001$). They also demonstrated significant longitudinal growth from 2 to 6 months (2 months, 22.3 ± 1.2 mm; 6 months, 26.0 ± 2.0 mm; $P = .03$).

In Vivo and Ex Vivo ^{99m}Tc-RP805 SPECT/CT

In vivo SPECT/CT demonstrated an increase in ^{99m}Tc-RP805 activity within the region of the IVC graft (Figure 3). Quantitative analysis of the ex vivo SPECT/CT images demonstrated greater ^{99m}Tc-RP805 activity within the TEVG than in the adjacent native IVC and significantly greater relative tracer uptake in the unseeded than in the seeded grafts (TEVG/native vessel, unseeded, 2.8 ± 0.4; seeded, 1.8 ± 0.3; $P = .03$; Figure 4).

Histologic Examination

Histologic examination was performed on the TEVG and native IVC tissue at 6 months after implantation to assess neotissue cellularity and the presence of collagen, glycosaminoglycans, and elastic fiber formation (Figure 5). Tissue staining with Masson's trichrome and hematoxylin and eosin demonstrated that the polymer had degraded by 6 months and had subsequently been replaced by a collagen-dominated neotissue. Alcian blue staining suggested increased glycosaminoglycan content in the seeded graft neotissues compared with the unseeded, with the glycosaminoglycans inhomogeneously distributed in the unseeded grafts (Figure 5, *B*). Elastica van Gieson staining demonstrated mild, but comparable, elastic fiber formation between the seeded and unseeded groups, with both remaining inferior to the native IVC (Figure 5).

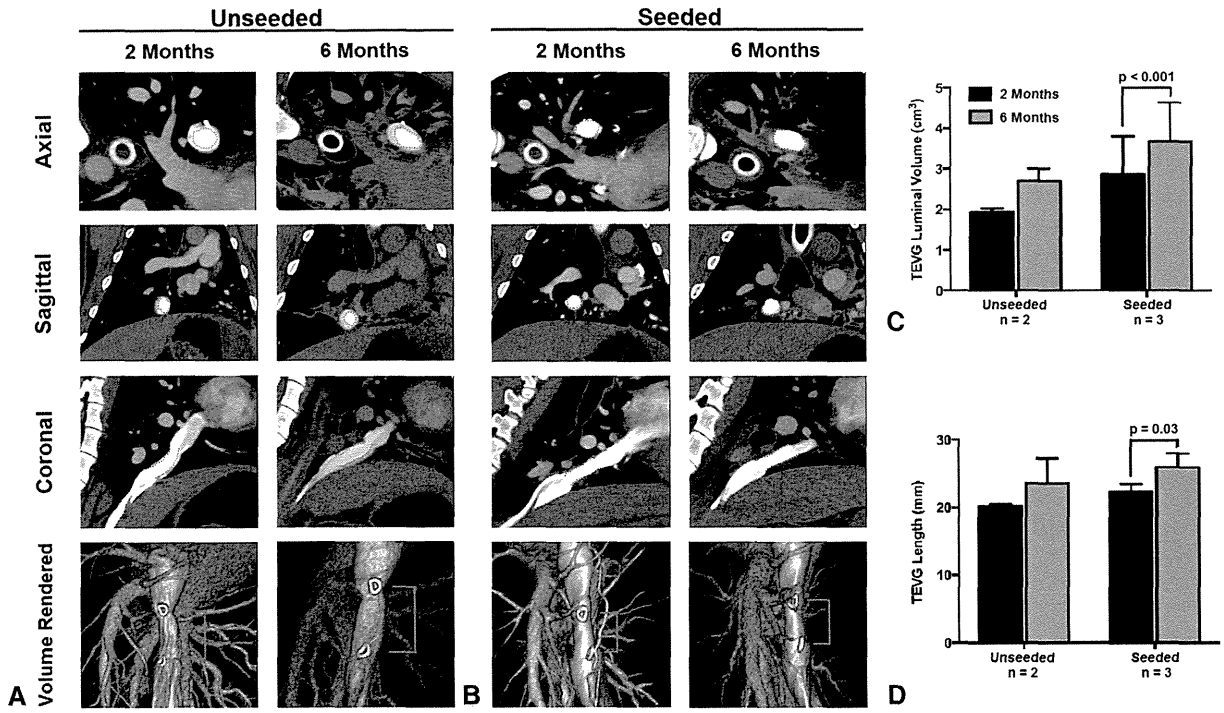

FIGURE 2. In vivo computed tomography angiography at 2 and 6 months after implantation of (A) an unseeded and (B) a seeded scaffold demonstrating graft patency (lumen indicated by red markers). Serial quantification of computed tomography angiography revealed significant increases in tissue engineered vascular graft (*TEVG*) (C) luminal volume and (D) length in seeded grafts.

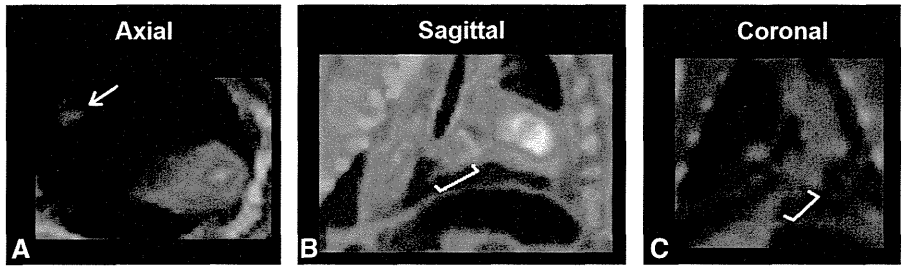

FIGURE 3. Increased technetium-99m–labeled RP805 activity was observed in the blood pool and region of inferior vena cava graft implantation (*yellow marker*) in (A) axial, (B) sagittal, and (C) coronal views.

Biochemical Analysis

No significant differences were observed in the collagen content within the seeded (n = 3, 65.2 ± 47.8 μg/mg) and unseeded (n = 2, 110.0 ± 11.8 μg/mg) TEVGs. The glycosaminoglycan content was significantly greater in the seeded TEVG group (n = 3, 6.5 ± 0.3 μg/mg) than in the unseeded TEVG group (n = 2, 4.1 ± 0.8 μg/mg; $P = .01$).

DISCUSSION

In the present study, we have demonstrated the feasibility of targeted SPECT/CT for the quantitative assessment of MMP activity within surgically implanted IVC interposition grafts with complementary serial evaluation of the graft morphologic changes using in vivo CT angiography. We used a previously validated lamb model of IVC graft implantation,[5] and the density centrifugation technique for isolation of BM-MNCs met the same criteria for scaffold cell attachment implemented in our ongoing clinical trial.[3] All grafts were patent at 2 and 6 months after implantation, with the seeded grafts demonstrating significant luminal and longitudinal growth (Figure 2). Significantly greater MMP activity was found in the grafts compared with the native IVC tissue at 6 months after implantation, with significantly greater MMP activity in the unseeded than in the seeded grafts (Figure 4). The elevated MMP activity in the grafts might have been related to ongoing neotissue formation that persisted at a greater level in the unseeded graft scaffolds at 6 months. The combined imaging techniques of CT angiography and hybrid SPECT/CT offer a potentially novel approach for the noninvasive, serial evaluation of ongoing graft remodeling and neotissue formation in tissue-engineered grafts.

Previous studies from our laboratory have indicated that neotissue formation occurs by way of an early inflammatory-mediated phase of vascular remodeling as the polymeric scaffold degrades.[20-22] The balance of the production and removal of structurally significant ECM constituents (eg, collagen, elastin, glycosaminoglycans) and the degradation of the implanted graft scaffold will dictate the vascular neotissue evolution. MMPs play an important role in this balance. Therefore, monitoring MMP activity could provide valuable information related to the status of neotissue development in the setting of TEVG implantation. Two previous studies have quantified MMP activity within TEVGs implanted as IVC interposition grafts; however, these studies required histologic evaluation of the explanted neotissue.[6,7] In the present study, we sought to evaluate the feasibility of the noninvasive assessment of MMP activity in a clinically relevant large animal model of TEVG implantation. We

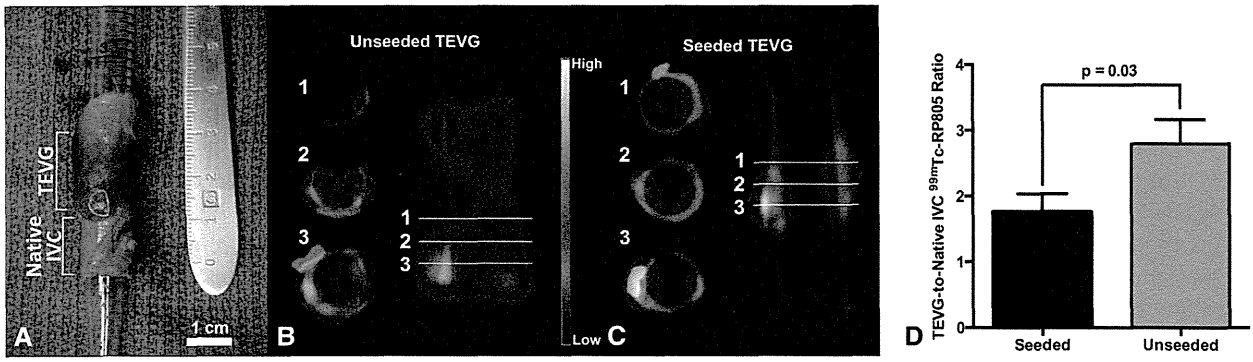

FIGURE 4. Ex vivo single photon emission computed tomography/computed tomography (SPECT/CT) imaging and quantification. A, Representative sample of explanted tissue engineered vascular graft (*TEVG*) and native inferior vena cava (*IVC*) tissue before ex vivo SPECT/CT imaging. SPECT/CT demonstrated heterogeneous uptake of technetium-99m–labeled RP805 (*^{99m}Tc-RP805*) in the graft, illustrated by representative cross sections of the vessel wall in both (B) unseeded and (C) seeded grafts. D, Significantly greater matrix metalloproteinase activity was seen in the unseeded than in the seeded grafts.

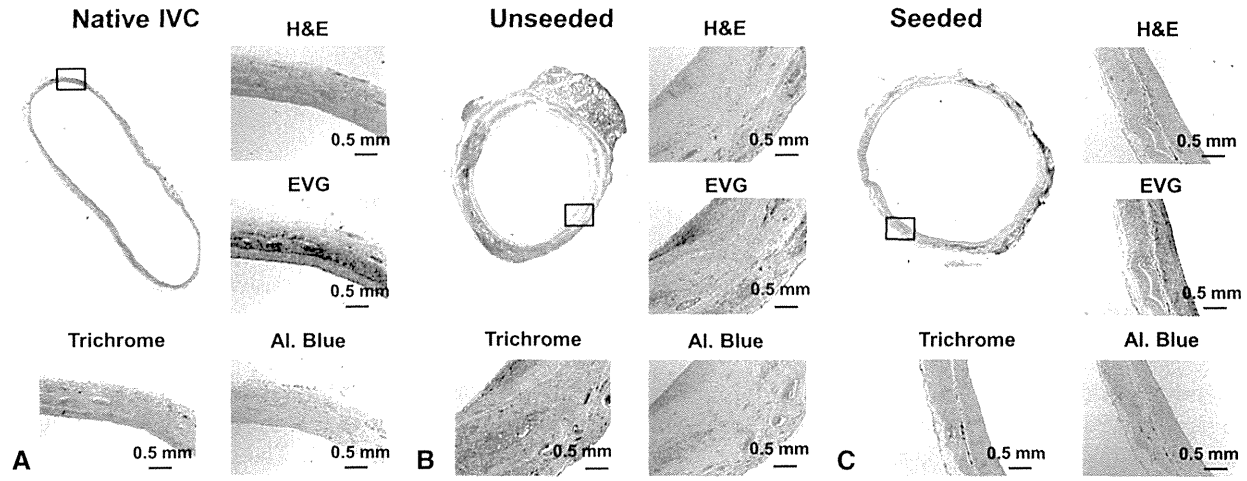

FIGURE 5. Hematoxylin and eosin (*H&E*), elastica van Gieson (*EVG*), Masson's trichrome (*trichome*), and Alcian blue (*Al. Blue*) staining of (A) native inferior vena cava (*IVC*), (B) unseeded tissue engineered vascular (TEVG) at 6 months, and (C) seeded TEVGs at 6 months. The implanted scaffolds had completely degraded within 6 months and had been replaced by collagen-dominated neotissue (B and C). Elastic fiber formation was comparable in the TEVGs but appeared suboptimal compared with the native IVC (A). Alcian blue staining demonstrated a greater amount of glycosaminoglycans in the seeded than in the unseeded TEVGs.

CHD

observed elevated MMP activity within the region of TEVG implantation at 6 months after implantation using in vivo SPECT/CT (Figure 3) of a broad-spectrum MMP-targeted radiotracer (^{99m}Tc-RP805). Although increased radiotracer activity was observed with in vivo SPECT/CT imaging, it was clear that much of this activity remained in the blood pool during the point of image acquisition at 1 hour after radiotracer injection, complicating the quantification of MMP activity in the graft at this early point after radiotracer injection (Figure 3). Improved in vivo localization and quantification of ^{99m}Tc-RP805 in the vascular wall might be achieved in future studies with the incorporation of a later image acquisition time (2-4 hours after radiotracer injection), as indicated by previous attempts at SPECT/CT vascular imaging of MMP activity.[11,13] Additionally, in vivo SPECT/CT imaging was not performed with cardiac gating, limiting the ability to quantify local MMP activity within the region of TEVG implantation.

Although limitations were present with in vivo SPECT/CT imaging that prevented quantification of TEVG radiotracer uptake, the MMP activity was quantified in TEVGs and native IVCs using ex vivo SPECT/CT imaging. Significant differences in MMP activity were found between the unseeded and seeded TEVGs at 6 months (Figure 4). Previous investigation in our laboratory has demonstrated the importance of cell seeding in the TEVG remodeling process and identified greater rates of stenosis in the unseeded than in the seeded scaffolds[23]; however, no evidence of aneurysm or stenosis was apparent in the unseeded or seeded scaffolds in the present study. Serial in vivo CT angiography demonstrated significant luminal and longitudinal growth in the seeded scaffolds from 2 to 6 months (Figure 2). This noted growth of TEVGs in the present study is consistent with previously reported results from our laboratory that identified serial changes in TEVG growth using magnetic resonance angiography in juvenile lambs.[5] The patterns of longitudinal growth measured by CT angiography suggest that implanted scaffolds will have biodegraded by 6 months and allowed for growth of newly formed neotissue within juvenile lambs that nearly doubled in weight during the 6-month study period (implantation weight, 22.4 ± 2.3 kg; 6-month weight, 42.7 ± 4.3 kg).

Histologic evaluation of the TEVG tissue at 6 months after implantation confirmed graft scaffold degradation and subsequent replacement by a collagen-dominant neotissue (Figure 5). Although no significant differences in collagen content were identified on biochemical analysis, the lower collagen content and increased MMP activation in the TEVGs than in the native IVC tissue suggests that ECM remodeling continued at 6 months after implantation and that the neotissue was still actively remodeling. Elastica-van Gieson staining demonstrated mild, but comparable, elastic fiber formation between the seeded and unseeded neotissue (Figure 5), although both TEVG groups remained inferior to the native IVC tissue. These histologic observations have indicated continued ECM remodeling that corresponds with the SPECT/CT findings of increased MMP activity at 6 months after TEVG implantation. Improved in vivo SPECT/CT imaging for the noninvasive assessment of MMP activity should greatly facilitate our understanding of the period associated with neotissue formation and enhance the application of tissue engineering within the cardiovascular system.

Study Limitations

A small number of lambs were used in the present study. Although these numbers were sufficient for a feasibility study, future investigations with a greater number of implantations will be necessary to increase the statistical power and evaluate the full potential of noninvasive imaging of MMPs in vascular grafts. Additionally, in vivo SPECT imaging was not optimized for localization and quantification of MMP activity. SPECT imaging protocols that incorporate cardiac gating and later acquisition times after radiotracer injection should provide improved localization of radiotracer activity and allow for noninvasive in vivo quantification of MMP activity within TEVGs. Although the present study evaluated the feasibility of noninvasive imaging of MMP activity for the detection of ongoing TEVG remodeling, immunohistochemistry was not performed. Such an analysis might have provided additional insight into the presence of specific MMPs within the neotissue at 6 months after implantation. Future investigations targeted at the TEVG remodeling process could greatly benefit from correlative immunohistochemistry findings to validate the noninvasive molecular imaging findings.

CONCLUSIONS

The present study has demonstrated the feasibility of targeted SPECT/CT imaging of MMP activity within TEVGs implanted in a growing large animal model. The ability to noninvasively assess MMP activity within TEVGs in vivo could provide a unique opportunity to evaluate the underlying mechanisms regulating the transition from TEVG to neovessel and might assist with improved translation of tissue engineering into clinical practice.

The authors would like to thank Christi Hawley for technical assistance with animal care and Yongjie Miao for consultation related to the statistical analyses. The authors would also like to thank Lantheus Medical Imaging, Inc, for supplying the RP805 compound used for SPECT imaging.

References

1. Shinoka T, Ikada Y, Imai Y. Transplantation of a tissue-engineered pulmonary artery. *N Engl J Med*. 2001;344:532-3.
2. Hibino N, McGillicuddy E, Matsumura G, Ichihara Y, Naito Y, Breuer C, et al. Late-term results of tissue-engineered vascular grafts in humans. *J Thorac Cardiovasc Surg*. 2010;139:431-6.
3. Vogel G. Mending the youngest hearts. *Science*. 2011;333:1088-9.
4. Shin'oka T, Matsumura G, Hibino N, Naito Y, Watanabe M, Konuma T, et al. Midterm clinical result of tissue-engineered vascular autografts seeded with autologous bone marrow cells. *J Thorac Cardiovasc Surg*. 2005;129:1330-8.
5. Brennan MP, Dardik A, Hibino N, Roh JD, Nelson GN, Papademitris X, et al. Tissue-engineered vascular grafts demonstrate evidence of growth and development when implanted in a juvenile animal model. *Ann Surg*. 2008;248:370-7.
6. Naito Y, Williams-Fritze M, Duncan DR, Church SN, Hibino N, Madri JA, et al. Characterization of the natural history of extracellular matrix production in tissue-engineered vascular grafts during neovessel formation. *Cells Tissues Organs*. 2011;195:60-72.
7. Cummings I, George S, Kelm J, Schmidt D, Emmert MY, Weber MY, et al. Tissue-engineered vascular graft remodeling in a growing lamb model: expression of matrix metalloproteinases. *Eur J Cardiothorac Surg*. 2012;41:167-72.
8. Lancelot E, Amirbekian V, Brigger I, Raynaud JS, Ballet S, David C, et al. Evaluation of matrix metalloproteinases in atherosclerosis using a novel noninvasive imaging approach. *Arter Thromb Vasc Biol*. 2008;28:425-32.
9. Hyafil F, Vucic E, Cornily J-C, Sharma R, Amirbekian V, Blackwell F, et al. Monitoring arterial wall remodelling in atherosclerotic rabbits with a magnetic resonance imaging contrast agent binding to matrix metalloproteinases. *Eur Hear J*. 2011;32:1561-71.
10. Haider N, Hartung D, Fujimoto S, Petrov A, Kolodgie FD, Virmani R, et al. Dual molecular imaging for targeting metalloproteinase activity and apoptosis in atherosclerosis: molecular imaging facilitates understanding of pathogenesis. *J Nucl Cardiol*. 2009;16:753-62.
11. Fujimoto S, Hartung D, Oshima S, Edwards DS, Zhou J, Yalamanchili P, et al. Molecular imaging of matrix metalloproteinase in atherosclerotic lesions: resolution with dietary modification and statin therapy. *J Am Coll Cardiol*. 2008;52:1847-57.
12. Razavian M, Tavakoli S, Zhang J, Nie L, Dobrucki LW, Sinusas AJ, et al. Atherosclerosis plaque heterogeneity and response to therapy detected by in vivo molecular imaging of matrix metalloproteinase activation. *J Nucl Med*. 2011;52:1795-802.
13. Zhang J, Nie L, Razavian M, Ahmed M, Dobrucki LW, Asadi A, et al. Molecular imaging of activated matrix metalloproteinases in vascular remodeling. *Circulation*. 2008;118:1953-60.
14. Tavakoli S, Razavian M, Zhang J, Nie L, Marfatia R, Dobrucki LW, et al. Matrix metalloproteinase activation predicts amelioration of remodeling after dietary modification in injured arteries. *Arter Thromb Vasc Biol*. 2011;31:102-9.
15. Sahul ZH, Mukherjee R, Song J, McAteer J, Stroud RE, Dione DP, et al. Targeted imaging of the spatial and temporal variation of matrix metalloproteinase activity in a porcine model of postinfarct remodeling: relationship to myocardial dysfunction. *Circ Cardiovasc Imaging*. 2011;4:381-91.
16. Su H, Spinale FG, Dobrucki LW, Song J, Hua J, Sweterlitsch S, et al. Noninvasive targeted imaging of matrix metalloproteinase activation in a murine model of postinfarction remodeling. *Circulation*. 2005;112:3157-67.
17. Hjortnaes J, Gottlieb D, Figueiredo J-L, Melero-Martin J, Kohler RH, Bischoff J, et al. Intravital molecular imaging of small-diameter tissue-engineered vascular grafts in mice: a feasibility study. *Tissue Eng*. 2010;16:597-607.
18. Udelsman B, Hibino N, Villalona G, McGillicuddy E, Neiponice A, Sakamoto Y, et al. Development of an operator-independent method for seeding tissue-engineered vascular grafts. *Tissue Eng Part C*. 2011;17:731-6.
19. Chan C, Dey J, Sinusas AJ, Liu C. Improved image reconstruction for dedicated cardiac SPECT with truncated projections. *J Nucl Med*. 2012;53(Suppl):105.
20. Roh JD, Sawh-Martinez R, Brennan MP, Jay SM, Devine L, Rao DA, et al. Tissue-engineered vascular grafts transform into mature blood vessels via an inflammation-mediated process of vascular remodeling. *Proc Natl Acad Sci U S A*. 2010;107:4669-74.
21. Hibino N, Villalona G, Pietris N, Duncan DR, Schoffner A, Roh JD, et al. Tissue-engineered vascular grafts form neovessels that arise from regeneration of the adjacent blood vessel. *FASEB J*. 2011;25:2731-9.
22. Roh JD, Nelson GN, Brennan MP, Mirensky TL, Yi T, Hazlett TF, et al. Small-diameter biodegradable scaffolds for functional vascular tissue engineering in the mouse model. *Biomaterials*. 2008;29:1454-63.
23. Hibino N, Yi T, Duncan DR, Rathore A, Dean E, Naito Y, et al. A critical role for macrophages in neovessel formation and the development of stenosis in tissue-engineered vascular grafts. *FASEB J*. 2011;25:4253-63.

TEC-2014-0442-ver9-Kurobe_1P
Type: research-article

TISSUE ENGINEERING: Part C
Volume 00, Number 00, 2014

DOI: 10.1089/ten.tec.2014.0442

Comparison of the Biological Equivalence of Two Methods for Isolating Bonemarrow Mononuclear Cells for Fabricating Tissue-Engineered Vascular Grafts

AU1 ▶ Hirotsugu Kurobe, MD, PhD,[1,*] Shuhei Tara, MD, PhD,[1,*] Mark W. Maxfield, MD,[2] Kevin A. Rocco, MS,[2] Paul S. Bagi, BA,[2] Tai Yi, MD, MS,[1] Brooks V. Udelsman, MD,[2] Ethan W. Dean, MD,[2] Ramak Khosravi, BA,[2] Heather M. Powell, PhD,[3] Toshiharu Shinoka, MD, PhD,[1,3] and Christopher K. Breuer, MD[1,3]

Our approach for fabricating tissue-engineered vascular grafts (TEVG), applied in the surgical management of congenital heart disease, is accomplished by seeding isolated bone marrow-derived mononuclear cells (BM-MNCs) onto biodegradable scaffolds. The current method used for isolation of BM-MNCs is density centrifugation in Ficoll. This is a time-consuming, labor-intensive, and operator-dependent method. We previously demonstrated that a simpler, faster, and operator-independent method for isolating BM-MNCs using a filter elution technique was feasible. In this study, we compare the use of each technique to determine if the BM-MNCs isolated by the filtration elution method are biologically equivalent to BM-MNCs isolated using density centrifugation. Scaffolds were constructed from a nonwoven poly(glycolic acid) fiber mesh coated with 50:50 poly(L-lactide-co-ε-caprolactone) sealant. BM-MNCs were isolated from the bone marrow of syngeneic C57BL/6 mice by either density centrifugation with Ficoll or filtration (Ficoll vs. Filter), then statically seeded onto scaffolds, and incubated overnight. The TEVG were implanted in 10-week-old C57BL/6 mice ($n=23$ for each group) as inferior vena cava interposition grafts and explanted at 14 days for analysis. At 14 days after implantation, there were no significant differences in graft patency between groups (Ficoll: 87% vs. Filter: 78%, $p=0.45$). Morphometric analysis by hematoxylin and eosin staining showed no difference of graft luminal diameter or neointimal thickness between groups (luminal diameter, Ficoll: $620.3\pm82.9\,\mu m$ vs. Filter: $633.3\pm131.0\,\mu m$, $p=0.72$; neointimal thickness, Ficoll: $37.9\pm7.8\,\mu m$ vs. Filter: $37.9\pm11.2\,\mu m$, $p=0.99$). Histologic examination demonstrated similar degrees of cellular infiltration and extracellular matrix deposition, and endothelial cell coverage on the luminal surface, in either group. Macrophage infiltration showed no difference in the number of F4/80-positive cells or macrophage phenotypes between the two experimental groups (Ficoll: 2041 ± 1048 cells/mm^2 vs. Filter: 1887 ± 907.7 cells/mm^2, $p=0.18$). We confirmed the biological equivalence of BM-MNCs, isolated using either density centrifugation or filtration, for making TEVG.

Introduction

CURRENT SURGICAL MANAGEMENT of congenital heart disease involves the use of synthetic vascular grafts, an approach that is limited by the absence of graft growth, high incidence of graft thrombosis, development of graft stenosis, ectopic calcification, and risk of infection.[1] To address the shortcomings of currently available synthetic grafts, tissue engineering techniques have emerged as a means of creating biologically active blood vessels: tissue-engineered vascular grafts (TEVG). TEVG offer the potential for surgeons to implant grafts that are capable of growth, remodeling, and repair. We have successfully implanted TEVG in humans with congenital heart defects.[2] Long-term follow-up has now shown that TEVG are safe and effective to use in pediatric patients.[3]

We utilize bone marrow-derived mononuclear cells (BM-MNCs) for cell seeding, which is a crucial step in fabricating our TEVG. The use of BM-MNCs instead of primary somatic cells (mesenchymal stromal cells, endothelial cells, or smooth muscle cells) eliminated the need for cell expansion in culture *ex vivo*, which decreases the risk of

[1]Nationwide Children's Hospital, Columbus, Ohio.
[2]Yale University School of Medicine, New Haven, Connecticut.
[3]The Ohio State University, Columbus, Ohio.
*These two authors contributed equally to this work.

◀ AU2

contamination and minimizes the amount of tissue needed to create the TEVG. However, current techniques for the construction of TEVG use density centrifugation as a means of isolating BM-MNCs and are limited by the risk of bacterial contamination, loss of cell viability, and need for a specialized clean room.[4] The development of simpler, more rapid, and operator-independent methods for manufacturing TEVG using closed disposable systems could overcome these disadvantages and facilitate more widespread use of TEVG products. We previously demonstrated the feasibility of a novel filtration system to isolate BM-MNCs from human bone marrow[5] and applied this technique to a closed disposable system for construction of TEVG by using an ovine model.[6]

In the present study, we isolated BM-MNCs in a murine model using two different methods: the conventional density centrifugation technique with Ficoll and the new filtration system. We then seeded the isolated BM-MNCs onto biodegradable scaffolds and then implanted these TEVG as inferior vena cava (IVC) interposition grafts in C57BL/6 mice. The objective of this study is to evaluate tissue remodeling as a means of assessing biological equivalence between the two methods in the construction of TEVG.

Materials and Methods

Scaffolds

Scaffolds were constructed using a dual cylinder chamber molding system from a nonwoven poly(glycolic acid) fiber mesh (Biomedical Structures, Warwick, RI) coated with a 50:50 copolymer sealant solution of poly(L-lactide-co-ε-caprolactone) (Absorbable Polymers International, Birmingham, AL), as previously described.[7,8] Scanning electron microscope images of scaffolds are shown in Figure 3A. Each scaffold was 4 mm in length and 0.9 mm in diameter.

BM-MNC preparation and seeding onto scaffolds

BM-MNCs were isolated from bone marrow of CB57BL/6 mice by using two techniques: density centrifugation in Ficoll and filtration (Ficoll vs. Filter). For the density centrifugation group, after bone marrow harvest, BM-MNCs were isolated by centrifugation for 30 min with Histopaque-1083 (Sigma, St. Louis, MO). After washing with phosphate-buffered saline (PBS), BM-MNCs were diluted with RPMI 1640 (Sigma).[8] For the filtration group, isolation of BM-MNCs was performed as described previously.[6] Briefly, the volume of bone marrow plus RMPI 1640 was increased to 15 mL and transferred to an initial chamber using a syringe; this was filtered by a simple gravitational flow using a commercially available cell harvest filter (Pall Corporation, Port Washington, NY). After washing the filter media with PBS twice to reduce contamination by red blood cells, BM-MNCs were recovered by back-flushing the filter with 6 mL of sterile 10% dextran 40/saline solution. The collected solution was centrifuged and the resulting pellet was diluted with RPMI 1640. Finally, 1.0×10^6 MNCs were prepared by both methods. Also, grafts were seeded by pipetting a concentrated cell suspension through the lumen of the scaffold. Cell-seeded grafts were preconditioned in a CO_2 incubator at 37°C for 18–24 h in 1 mL of RPMI 1640 under sterile conditions.[8]

Cell counts were performed after BM-MNC isolation in each group, and viability of these cells was obtained by trypan blue staining with manual cell count. The cellularity of the seeded scaffolds after overnight incubation was determined by measuring the DNA content with a PicoGreen detection assay (Molecular Probes, Eugene, OR).[4]

Animal model and surgical implantation

All animals received humane care in compliance with the National Institutes of Health Guide for the Care and Use of Laboratory Animals. The Institutional Animal Care and Use Committee at Yale University approved the use of animals and all procedures described in this study. C57BL/6 mice were purchased from Jackson Laboratories (Bar Harbor, ME).

TEVG were implanted in 10-week-old CB57BL/6 mice ($n = 23$ for each group) as IVC interposition grafts, using a standard microsurgical technique as previously described.[7,8] Animals were sacrificed at 14 days and grafts were explanted for analysis after the saline perfusion.

Serial monitoring of TEVG by ultrasound

Ultrasonography (Vevo Visualsonics 770; Visualsonics, Toronto, ON) was used to serially monitor patency of grafts at 3, 7, and 14 days after implantation. Before ultrasonography, mice were anesthetized with 1.5% inhaled isoflurane. The graft luminal diameter was determined sonographically,

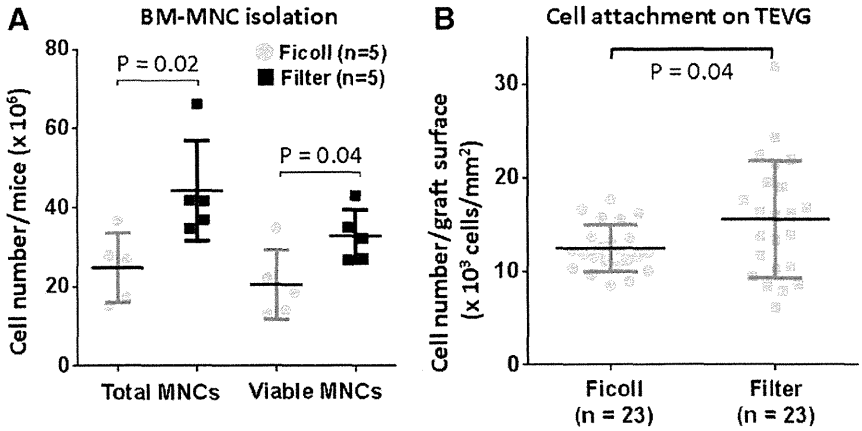

FIG. 1. Comparison of isolated bone marrow-derived mononuclear cells (BM-MNCs) and cell attachment after seeding. **(A)** Total and viable cell count of BM-MNCs was performed by trypan blue staining with manual cell count. The filter method isolated significantly more BM-MNCs in both total and viable cells. Data were evaluated by Student *t* test. **(B)** Cell attachment on the graft was evaluated by PicoGreen DNA quantification after overnight incubation. The number of attached cells in the filter group was higher than that in the Ficoll group. Data were evaluated by Welch's *t* test.

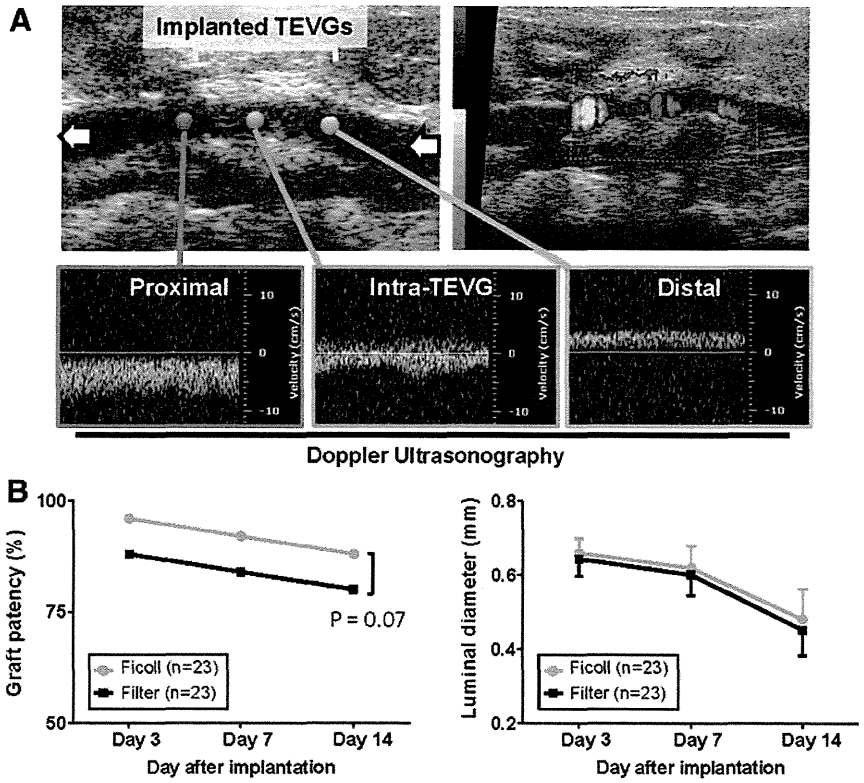

FIG. 2. Serial monitoring of graft patency and luminal diameter by ultrasonography. **(A)** Representative images of ultrasound. The graft luminal diameter was determined sonographically and patency was determined by measuring flow velocity proximal and distal to the graft. **(B)** Serial monitoring by ultrasound demonstrated no difference in graft patency and luminal diameter between groups at each time point. Color images available online at www.liebertpub.com/tec

and patency was determined by measuring Doppler flow velocity proximal and distal to the graft (Fig. 2A).

Histology and immunohistochemistry

Explanted grafts at 14 days after implantation were fixed in 4% paraformaldehyde, embedded in paraffin, sliced (5 μm sections), and stained with hematoxylin and eosin (HE), Masson's trichrome, Elastica van Gieson, Alcian Blue, and von Kossa. The adventitia, media, and intima were manually identified and measured with ZEN lite (Carl Zeiss, Oberkochen, Germany) on HE staining histologically, and patency was defined as >50% in luminal diameter compared to graft at the time of implantation (Fig. 3B).

Identification of smooth muscle cells, endothelial cells, matrix metalloproteinase-2 (MMP-2), and macrophages was done by immunohistochemical staining of paraffin-imbedded explant sections with the anti-SMA antibody (DAKO, Carpinteria, CA), anti-vWF (DAKO) antibody, anti-MMP-2 antibody (Millipore, Billerica, MA), anti-F4/80 antibody (DAKO), anti-iNOS antibody (Abcam, Cambridge, MA), and anti-CD206 antibody (Abcam), respectively. Primary antibody binding was detected using biotinylated immunoglobulin G (Vector, Burlingame, CA), and this was followed by the binding of streptavidin-horseradish peroxidase and color development with 3,3-diaminobenzidine.

Macrophages identified by positive F4/80 expression were quantified in explanted scaffolds. Two or three separate sections of each explant were stained with F4/80 and imaged at 400× magnification. Each section was divided into eight equal sections and nuclei were counted in three of those regions.

RNA extraction and reverse transcription quantitative polymerase chain reaction

Explanted grafts at 14 days after implantation were frozen in optimal cutting temperature compound (Sakura Finetek, Torrance, CA) and sectioned into twenty 30 μm sections. Total RNA was extracted and purified using the RNeasy mini kit (Qiagen, Valencia, CA) according to the manufacturer's instructions. Reverse transcription was performed using the High Capacity RNA-to-cDNA Kit (Applied Biosystems, Foster City, CA). All reagents and instrumentation for gene expression analysis were obtained from Applied Biosystems. Quantitative polymerase chain reaction (qPCR) was performed with a Step One Plus Real-Time PCR System using the TaqMan Universal PCR Master Mix Kit. Reference numbers for primers are as follows: itgam (Mm00434455_m1), CCR2 (Mm00438270_m1), ym1 (Mm00657889_mH), and HPRT (Mm00446968_m1). The results were analyzed using the comparative threshold cycle method, normalized with HPRT as an endogenous reference, and reported as relative values (ΔΔCT) to those of control native IVC

Statistical analysis

Our previous study and preliminary observation indicated that the patency rate at 2 weeks after the implantation was 70% for the traditional BM-MNC-seeded group and 30% for the unseeded group. According to these data, a power calculation by Fisher's exact probability test, with 0.05 of alpha-error and 0.8 of power, was completed to decide the sample number.

Numeric values are listed as mean with standard deviation. The number of experiments is shown in each case. Data

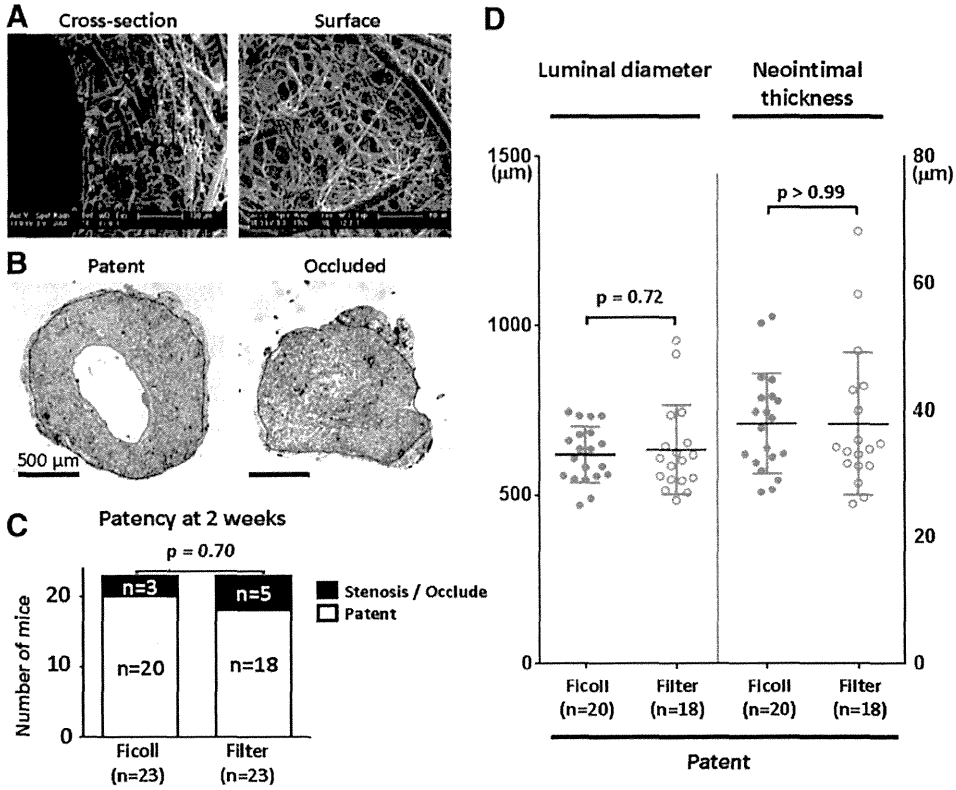

FIG. 3. Comparison of quantitative morphometric analysis of tissue-engineered vascular grafts (TEVG). (**A**) Representative scanning electron microscope images of scaffolds before cell seeding. (**B**) Representative hematoxylin and eosin (HE) staining images of patent and occluded TEVG. (**C**) The adventitia, media, and intima were manually identified and measured on HE staining, and patent was defined as greater than 50% in luminal diameter compared to graft at time of implantation. There was no statistical difference in patency of grafts at 2 weeks between the groups. Data were evaluated by Fisher's exact test. (**D**) Neither luminal diameter nor neointimal thickness differed between groups. Data were evaluated by Welch's *t* test. Color images available online at www.liebertpub.com/tec

of continuous variables with normal distribution were evaluated by Student's *t* test or by Welch's *t* test in instances when two groups had unequal variance. The nonparametric Mann–Whitney test was performed to detect significant difference of continuous variables with non-normal distributions. Fisher's exact test was used for dichotomous variables. *p* Values of <0.05 indicated statistical significance.

Results

Comparing isolation of MNCs

The number of total MNCs and viable MNCs after isolation from bone marrow cells using filtration was statistically higher than that using density centrifugation (total cells, Ficoll: $24.8\pm8.8\times10^6$/mouse vs. Filter: $44.3\pm12.6\times10^6$/mouse, $p=0.02$; viable cells, Ficoll: $20.6\pm8.7\times10^6$/mouse vs. Filter: $32.8\pm6.7\times10^6$/mouse, $p=0.04$, respectively; Fig. 1A). Evaluation of cell attachment onto seeded scaffolds by PicoGreen DNA assay showed a statistically significant difference in the number of cells after overnight incubation of scaffold between these two groups (Ficoll: $12.4\pm2.5\times10^3$/mm^2 vs. Filter: $15.5\pm6.3\times10^3$/mm^2, $p=0.04$; Fig. 1B).

Monitoring of TEVG by ultrasound

Serial ultrasonographic imaging demonstrated no difference in graft patency and luminal diameter between the density centrifugation and filtration groups, and these parameters gradually decreased in both groups during the observation period (Fig. 2B). While Figure 2B illustrates decreased graft patency in the filtration group at each time point, this difference was not statistically different. There was no aneurysm formation, hemorrhagic complications, or ectopic calcification in either group.

Quantitative morphometric analysis of TEVG

At 14 days after implantation, there was no difference between groups in terms of graft patency with the Ficoll group achieving 87% patency and the Filter group achieving 78% patency evaluated with HE staining ($p=0.70$; Fig. 3C). Morphometric analysis of patent grafts demonstrated no statistically significant difference in the luminal diameter (Ficoll: 620 ± 82.9 μm vs. Filter: 633 ± 131 μm, $p=0.72$) or neointimal thickness (Ficoll: 37.9 ± 7.8 μm vs. Filter: 37.9 ± 11.2 μm, $p>0.99$) (Fig. 3D).

Histological analysis of TEVG

HE staining of TEVG at 14 days after implantation revealed similarities in neovessel development, with similar degree of cellular infiltration within the TEVG, and no differences in cellular distribution or architecture between the two groups (Ficoll and Filter) (Fig. 4). Extracellular matrix stains using Masson's trichrome and Alcian blue stain displayed a robust deposition of collagen throughout TEVG in both groups (Fig. 4). There was no evidence of elastin in 14-day explants of both groups. The von Kossa stain revealed no instances of calcification in either group (Fig. 4). Poly(glycolic acid) fibers, which may appear as vacuoles or capillaries, still existed in the TEVG at the 14-day time point and caused nonspecific staining of both von Kossa and Alcian blue stain.

Smooth muscle cells, which were defined by immunohistochemical SMA staining, were primarily localized in the neointima of both experimental groups (Fig. 5, left). Endothelialization of the luminal surface was identified in TEVG in both groups by vWF staining (Fig. 5, middle). MMP-2 is integral to the remodeling process in TEVG and

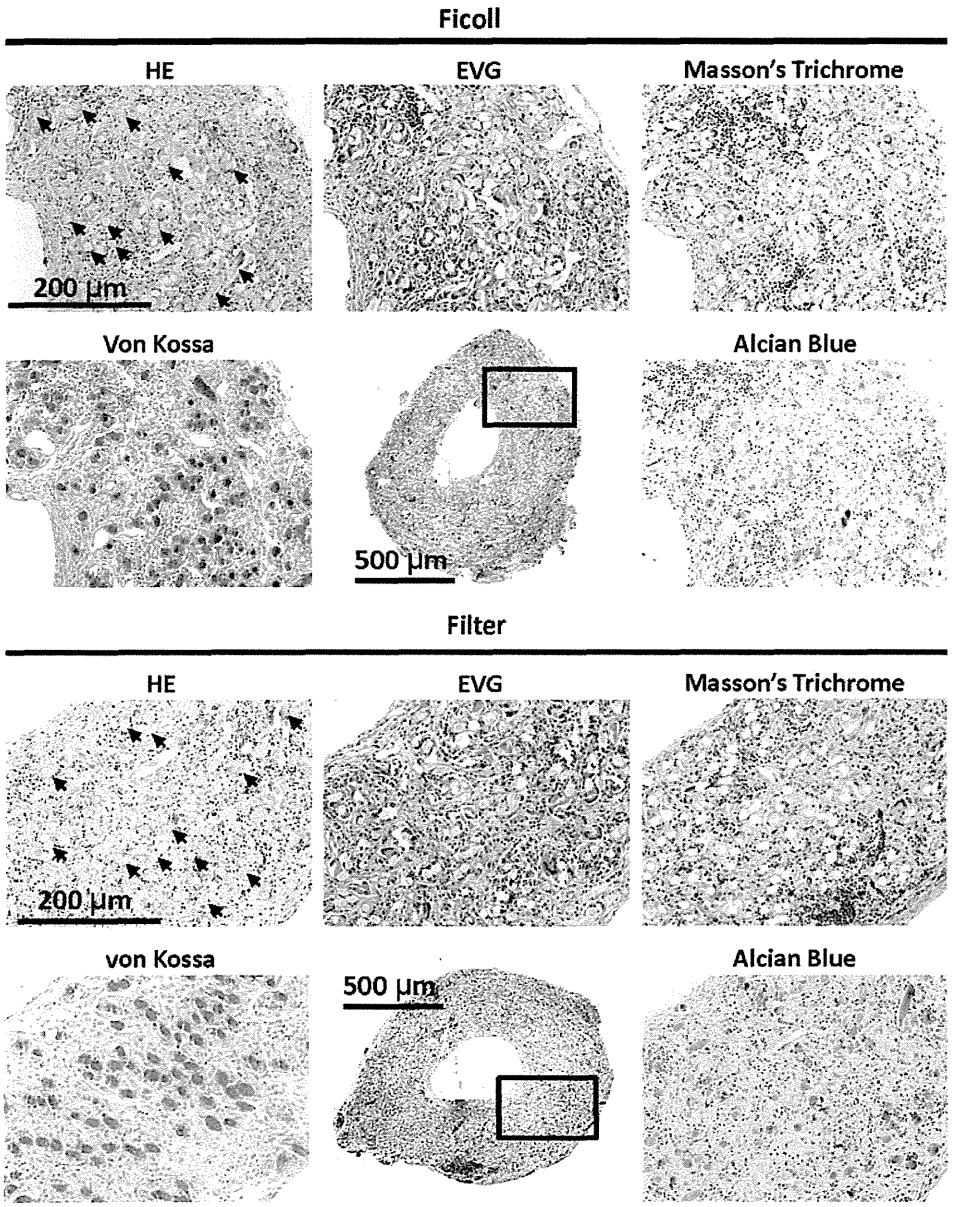

FIG. 4. Histological analysis of TEVG at 14 days after implantation. Histologic examination showed cellular infiltration into the TEVG, and robust deposition of collagen throughout the TEVG in both experimental groups, although there was no evidence of elastin. von Kossa stain revealed no instances of calcification in either group. Poly(glycolic acid) fibers, which may appear as vacuoles or capillaries, still existed in the TEVG and caused nonspecific staining of both von Kossa and Alcian blue stains. *Arrows* indicate representative remaining fibers on HE staining. Color images available online at www.liebertpub.com/tec ◀ AU7

peaks at 2 weeks after implantation in mice.[9] In the present study, MMP 2 was positive and similar between the two groups at 2 weeks after implantation (Fig. 5, right).

Macrophage analysis of TEVG

Immunohistochemical characterization with anti-F4/80 antibody demonstrated that macrophage infiltration of TEVG occurred in both groups (Fig. 6A, left). Staining for M1 and M2, which are the two major phenotypes of macrophage, in TEVG in both groups showed no difference between techniques of BM-MNC isolation (Fig. 6A, middle and right). Quantitation of the degree of macrophage infiltration showed no statistically significant difference in the number of F4/80-positive cells between the two experimental groups (Ficoll: 2041 ± 1048 cells/mm^2 vs. Filter: 1887 ± 907.7 cells/mm^2, $p = 0.18$; Fig. 6B). Gene expression of monocyte/macrophage marker (CD11b) evaluated by qPCR demonstrated that there was no statistical significance between two experimental groups in each time point "before seeding" and "14-day after implantation" (before seeding, Ficoll: 1.00 ± 0.60 vs. Filter: 1.38 ± 0.68, $p = 0.16$; 14-day after implantation, Ficoll: 1.0 ± 0.55 vs. Filter 1.03 ± 0.71, $p = 0.97$, respectively; Fig. 6C). Furthermore, there was no difference in macrophage phenotype (M1 and M2) evaluated by qPCR between groups at 14-day time point (M1, Ficoll: 1.00 ± 0.99 vs. Filter: 0.82 ± 0.67, $p = 0.67$; M2, Ficoll: 0.92 ± 0.67 vs. Filter 1.26 ± 1.30, $p = 0.52$, respectively; Fig. 6C).

F6 ▶

Discussion

In our previous studies, we demonstrated the importance of host-derived infiltrating macrophages on neovessel formation.[10,11] In studies evaluating vascular neotissue formation in TEVG in animals that were macrophage depleted using clodronate liposomes, we demonstrated that

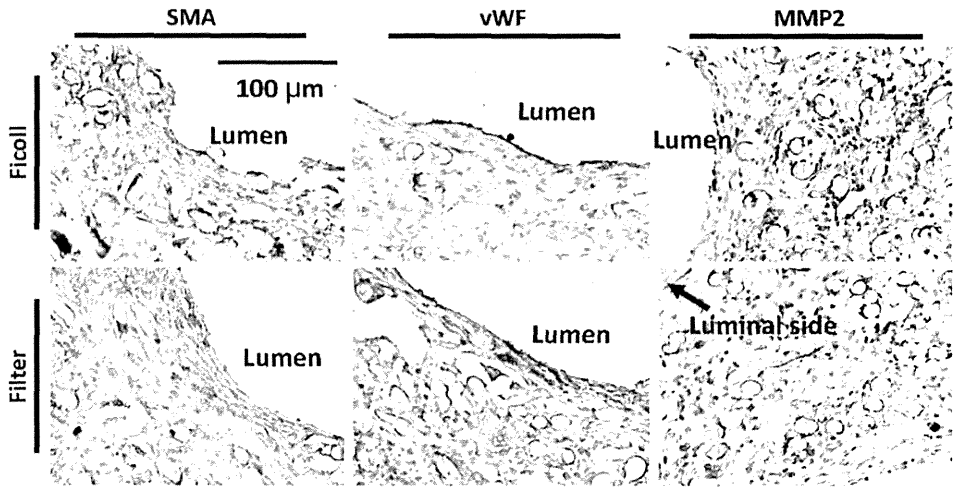

FIG. 5. Immunohistological analysis of TEVG at 14 days after implantation. (*Left*) Smooth muscle cells were shown mainly in neointima of both groups. (*Middle*) Endothelialization of the luminal surface was found to line the luminal surface of the TEVG by vWF staining. (*Right*) Matrix metalloproteinase (MMP)-2 was positive around the remaining fibers in both groups. There was no difference in these results between the two groups. Color images available online at www.liebertpub.com/tec

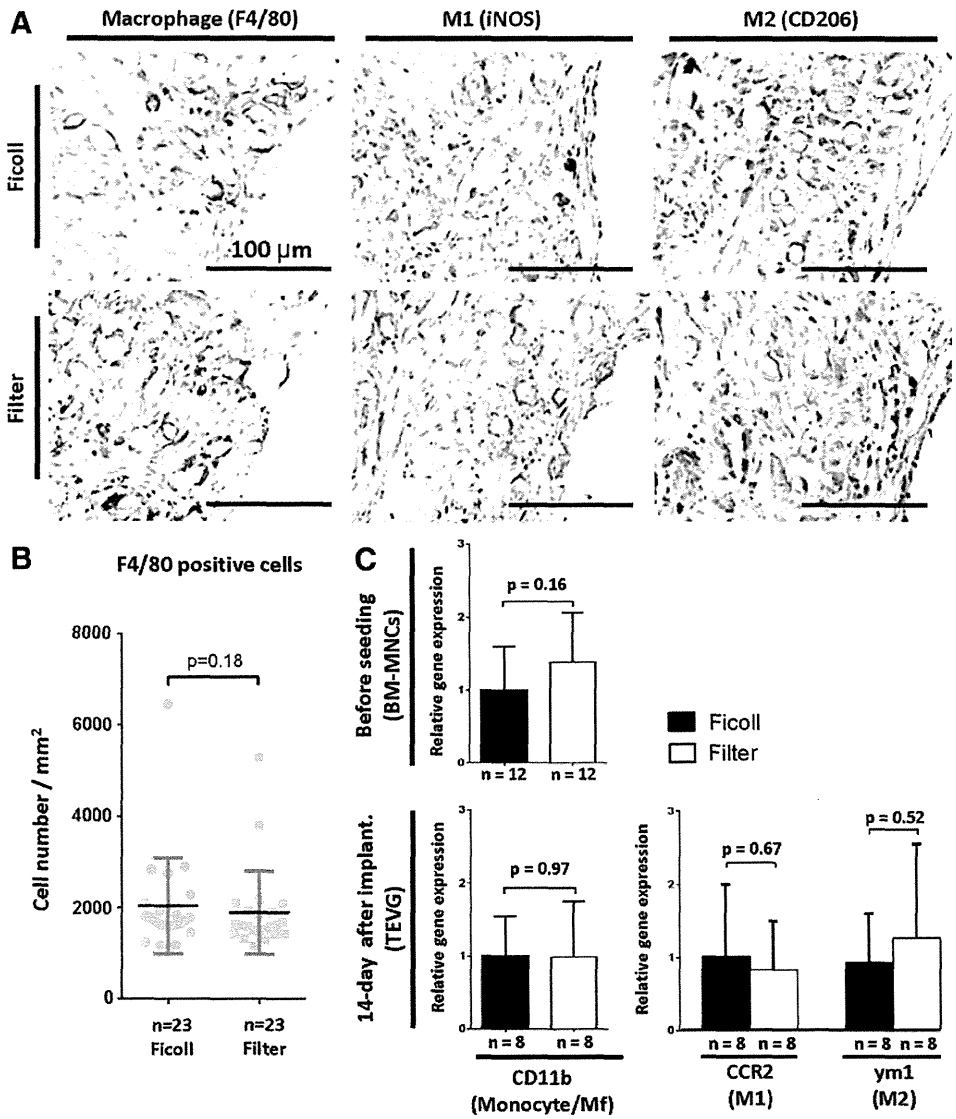

FIG. 6. Macrophage infiltration into TEVG evaluated by histological assessment and gene expression. **(A)** Representative images of immunohistochemical staining of F4/80 (entire macrophage), iNOS (M1 macrophage), and CD206 (M2 macrophage). **(B)** The number of macrophages in TEVG, defined by F4/80-positive cells, at 14 days after implantation showed no difference between groups. Data were evaluated by the Mann–Whitney test. **(C)**, Gene expression was analyzed by reverse transcription quantitative polymerase chain reaction using the ΔΔCT method. Gene expression of monocyte/macrophage marker (CD11b) demonstrated that there was no difference between the two experimental groups in each time point "before seeding" and "14 days after implantation" Furthermore, there was no difference in gene expression of macrophage phenotype (M1: iNOS and M2: CD206) between groups at 14-day time point. Data were evaluated by Student's *t* test. Color images available online at www.liebertpub.com/tec

macrophages are essential for vascular neotissue formation and we validated these findings using an inducible CD11b knockout mouse model.[11] In this same study, we discovered that the macrophages infiltrating patent TEVG demonstrated a shift away from the M1 phenotype, while the macrophages infiltrating stenotic TEVG demonstrated increased expression of M1 phenotypic markers. We have also previously demonstrated that cell seeding is not essential for vascular neotissue formation, but instead functions to improve patency by modulating the host inflammatory response to the TEVG scaffold by decreasing the number infiltrating macrophages and shifting the macrophage phenotype away from M1 through an as yet undetermined paracrine mechanism.[10,11] Thus, we postulate that measuring the degree of macrophage infiltration and characterizing the macrophage phenotype can serve as biomarkers to measure the biological function of the seeded cells in the TEVG.

In the present study, we evaluated and compared the biological activity of BM-MNC isolated using either our conventional density centrifugation method or our novel filtration elution method on vascular neotissue formation in TEVG. We demonstrated no difference in the biological activity on tissue remodeling in implanted TEVG seeded with BM-MNCs isolated using either technique. Specifically, we demonstrated no difference in the incidence of stenosis or the quality of the vascular neotissue. In addition, we demonstrated that the BM-MNCs induced the same degree of macrophage infiltration and M1 polarization despite previously demonstrated differences in the subpopulations of cells that comprise the BM-MNCs based on the method of separation.[5]

In the clinical arena, traditional methods of isolating BM-MNCs rely on density centrifugation, which is a time-consuming and labor-intensive process with a high degree of operator variability.[4] The filter-based method was originally used for isolating MNCs from peripheral blood.[12] Due to its success, we applied this technique to our method for construction of TEVG and demonstrated feasibility in isolating MNCs from human bone marrow as an alternative to conventional density centrifugation by showing morphologic equivalence in neovessel formation in the TEVG implantation model.[5] However, in that study, we used human bone marrow and implanted the BM-MNC-seeded TEVG in an immunodeficient SCID/bg mouse.[5] In the present study, we utilize autologous BM-MNCs for TEVG with implantation into immunocompetent wild-type CB57BL/6 mice and demonstrate biological equivalence of both methodologies in neotissue formation of smooth muscle cells and endothelial cells, both of which have been deemed essential to the structural and functional integrity of neovessels.[13,14]

In this study, the number of attached cells on scaffolds in the Filter group was higher than the Ficoll group after overnight incubation, and the viable cell number in the Filter group was higher than that in the Ficoll group. These results suggest that the filter method is less harsh compared to the density centrifugation method, in addition to being simpler, faster, and operator independent. Furthermore, our previous study demonstrated the difference in lymphocyte and monocyte populations in isolated cells between these two groups, and this fact might affect the number of attached cells on the scaffold and the viability of isolated cells. However, despite these differences, the two BM-MNC populations had a similar biological effect on TEVG formation.

The feasibility of using filter-based isolation of MNCs for fabricating TEVG was established by our previous study.[5] Furthermore, we demonstrated the safety and efficacy of using a closed system to create TEVG in a large animal model.[6] In this study, we demonstrated that despite differences in the BM-MNC isolated using either methodology, both BM-MNC populations exerted the same biologic effect and functionality as evidenced by similarities in the degree of cellular infiltration and formation of the TEVG.

Acknowledgments

The authors would like to thank Nancy Troiano, Rose Webb, and Christiane Coady of the Yale Core Center for Musculoskeletal Disorders for their technical expertise in processing murine TEVG tissue. Finally, they would also like to acknowledge Martin Smith from the Pall Corporation for his assistance in the design of the prototype for the closed disposable seeding system. The project described was supported by Award Number Grant UL1TR001070 from the National Center for Advancing Translational Sciences. The content is solely the responsibility of the authors and does not necessarily represent the official views of the National Center for Advancing Translational Sciences or the National Institutes of Health.

Disclosure Statement

C.K.B. and T.S. receive grant support from Gunze Ltd. (Kyoto, Japan). C.K.B. receives grant support from Pall Corp (NY). S.T. and H.K. were recipients of Banyu Fellowship from Banyu Life Science Foundation International (Tokyo, Japan) (H.K. in 2011 and S.T. in 2012). H.K. was recipient of fellowship from the Shinsenkai Imabari Daiichi Hospital (Ehime, Japan) in 2013.

References

1. Kurobe, H., Maxfield, M.W., Breuer, C.K., and Shinoka, T. Concise review: tissue-engineered vascular grafts for cardiac surgery: past, present, and future. Stem Cells Transl Med **1,** 566, 2012.
2. Shin'oka, T., Imai, Y., and Ikada, Y. Transplantation of a tissue-engineered pulmonary artery. N Engl J Med **344,** 532, 2001.
3. Hibino, N., McGillicuddy, E., Matsumura, G., Ichihara, Y., Naito, Y., Breuer, C., and Shinoka, T. Late-term results of tissue-engineered vascular grafts in humans. J Thorac Cardiovasc Surg **139,** 431, 2010.
4. Udelsman, B., Hibino, N., Villalona, G.A., McGillicuddy, E., Nieponice, A., Sakamoto, Y., Matsuda, S., Vorp, D.A., Shinoka, T., and Breuer, C.K. Development of an operator-independent method for seeding tissue-engineered vascular grafts. Tissue Eng Part C Methods **17,** 731, 2011.
5. Hibino, N., Nalbandian, A., Devine, L., Martinez, R.S., McGillicuddy, E., Yi, T., Karandish, S., Ortolano, G.A., Shin'oka, T., Snyder, E., and Breuer, C.K. Comparison of human bone marrow mononuclear cell isolation methods for creating tissue-engineered vascular grafts: novel filter system versus traditional density centrifugation method. Tissue Eng Part C Methods **17,** 993, 2011.
6. Kurobe, H., Maxfield, M.W., Naito, Y., Cleary, M., Stacy, M., Solomon, D., Rocco, K.A., Tara, S., Lee, A., Sinusas,

A., Snyder, E., Shinoka, T., and Breuer, C.K. Comparison of a closed system to a standard open technique for preparing tissue engineered vascular grafts. Tissue Eng Part C Methods 2014 (In press).
7. Roh, J.D., Nelson, G.N., Brennan, M.P., Mirensky, T.L., Yi, T., Hazlett, T.F., Tellides, G., Sinusas, A.J., Pober, J.S., Saltzman, W.M., Kyriakides, T.R., and Breuer, C.K. Small-diameter biodegradable scaffolds for functional vascular tissue engineering in the mouse model. Biomaterials **29,** 1454, 2008.
8. Lee, Y.U., Yi, T., Tara, S., Lee, A.Y., Hibino, N., Shinoka, T., and Breuer, C.K. Implantation of inferior vena cava interposition graft in mouse model. J Vis Exp **88,** e51632 [Epub ahead of print]; DOI: 10.3791/51632, 2014.
9. Naito, Y., Williams-Fritze, M., Duncan, D.R., Church, S.N., Hibino, N., Madri, J.A., Humphrey, J.D., Shinoka, T., and Breuer, C.K. Characterization of the natural history of extracellular matrix production in tissue-engineered vascular grafts during neovessel formation. Cells Tissues Organs **195,** 60, 2012.
10. Roh, J.D., Sawh-Martinez, R., Brennan, M.P., Jay, S.M., Devine, L., Rao, D.A., Yi, T., Mirensky, T.L., Nalbandian, A., Udelsman, B., Hibino, N., Shinoka, T., Saltzman, W.M., Snyder, E., Kyriakides, T.R., Pober, J.S., and Breuer, C.K. Tissue-engineered vascular grafts transform into mature blood vessels via an inflammation-mediated process of vascular remodeling. Proc Natl Acad Sci U S A **107,** 4669, 2010.
11. Hibino, N., Yi, T., Duncan, D.R., Rathore, A., Dean, E., Naito, Y., Dardik, A., Kyriakides, T., Madri, J., Pober, J.S., Shinoka, T., and Breuer, C.K. A critical role for macrophages in neovessel formation and the development of stenosis in tissue-engineered vascular grafts. FASEB J **25,** 4253, 2011.
12. Teleron, A.A., Carlson, B., and Young, P.P. Blood donor white blood cell reduction filters as a source of human peripheral blood-derived endothelial progenitor cells. Transfusion **45,** 21, 2005.
13. Vane, J.R., Anggard, E.E., and Botting, R.M. Regulatory functions of the vascular endothelium. N Engl J Med **323,** 27, 1990.
14. Wagenseil, J.E., and Mecham, R.P. Vascular extracellular matrix and arterial mechanics. Physiol Rev **89,** 957, 2009.

Address correspondence to:
Christopher K. Breuer, MD
Nationwide Children's Hospital
575 Children's Cross Roads
Columbus, OH 43215

E-mail: christopher.breuer@nationwidechildrens.org

Received: July 23, 2014
Accepted: November 5, 2014
Online Publication Date:

AUTHOR QUERY FOR TEC-2014-0442-VER9-KUROBE_1P

AU1: Please review all authors' surnames for accurate indexing citations.
AU2: Please provide the Department names in affiliations 1–3.
AU3: Figure citations are not in sequential order. Please check.
AU4: Please define SMA, vWF, and iNOS.
AU5: Please expand iNOS.
AU6: In Ref. 6, please mention the volume number and page range. If these are unavailable, please supply the article's full DOI number.
AU7: Please mention what box indicates in Figure 4 legend.

Atherosclerosis 237 (2014) 684–691

Contents lists available at ScienceDirect

Atherosclerosis

journal homepage: www.elsevier.com/locate/atherosclerosis

Well-organized neointima of large-pore poly(L-lactic acid) vascular graft coated with poly(L-lactic-co-ε-caprolactone) prevents calcific deposition compared to small-pore electrospun poly(L-lactic acid) graft in a mouse aortic implantation model

Shuhei Tara [a, 1], Hirotsugu Kurobe [a, 1], Kevin A. Rocco [b], Mark W. Maxfield [c], Cameron A. Best [a], Tai Yi [a], Yuji Naito [c], Christopher K. Breuer [a], Toshiharu Shinoka [a, d, *]

[a] Tissue Engineering Program and Surgical Research, Nationwide Children's Hospital, Columbus, OH, USA
[b] Department of Biomedical Engineering, Yale University, New Haven, CT, USA
[c] Department of Surgery, Yale University School of Medicine, New Haven, CT, USA
[d] Department of Cardiothoracic Surgery, The Heart Center, Nationwide Children's Hospital, Columbus, OH, USA

ARTICLE INFO

Article history:
Received 21 July 2014
Received in revised form
15 September 2014
Accepted 26 September 2014
Available online 17 October 2014

Keywords:
Atherosclerotic cardiovascular diseases
Calcification
Tissue engineering
Bioabsorbable grafts
Pore size
Electrospinning technique

ABSTRACT

Objective: Tissue engineering techniques have emerged that allow bioresorbable grafts to be implanted that restore function and transform into biologically active arteries. However, these implants are susceptible to calcification during the remodeling process. The objective of this study was to evaluate the role of pore size of bioabsorbable grafts in the development of calcification. **Methods**: Two types of grafts were prepared: a large-pore graft constructed of poly(L-lactic acid) (PLA) fibers coated with poly(L-lactide-co-ε-caprolactone) (PLCL) (PLA–PLCL), and a small-pore graft made of electrospun PLA nanofibers (PLA-nano). Twenty-eight PLA–PLCL grafts and twenty-five PLA-nano grafts were implanted as infrarenal aortic interposition conduits in 8-week-old female SCID/Bg mice, and followed for 12 months after implantation. **Results**: Large-pore PLA–PLCL grafts induced a well-organized neointima after 12 months, and Alizarin Red S staining showed neointimal calcification only in the thin neointima of small-pore PLA-nano grafts. At 12 months, macrophage infiltration, evaluated by F4/80 staining, was observed in the thin neointima of the PLA-nano graft, and there were few vascular smooth muscle cells (VSMCs) in this layer. On the other hand, the neointima of the PLA–PLCL graft was composed of abundant VSMCs, and a lower density of macrophages (F4/80 positive cells, PLA–PLCL; 68.1 ± 41.4/mm^2 vs PLA-nano; 188.3 ± 41.9/mm^2, $p = 0.007$). The VSMCs of PLA–PLCL graft expressed transcription factors of both osteoblasts and osteoclasts. **Conclusion**: These findings demonstrate that in mouse arterial circulation, large-pore PLA–PLCL grafts created a well-organized neointima and prevented calcific deposition compared to small-pore, electrospun PLA-nano grafts.

1. Introduction

Atherosclerotic cardiovascular diseases (CVD), including coronary heart disease, carotid artery stenosis, and peripheral arterial disease, is the leading cause of death or impaired quality of life for millions of individuals in the United States [1]. The most successful therapy for CVD is bypass surgery using autologous arteries and veins [2]. Unfortunately, many patients lack suitable donor tissue due to previous surgery or as a result of their underlying vascular disease. Synthetic vascular grafts like expanded polytetrafluoroethylene (Gore-Tex®), polyethylene terephthalate (Dacron®), and polyurethanes are employed in large caliber arteries where flow is high and resistance is low and have a history of long-term success [3]. However, current synthetic small diameter (<6 mm) grafts have not yet shown clinical efficacy due to poor patency as a result of thrombogenesis [4].

Tissue engineered vascular grafts (TEVG) offer the potential of a synthetic conduit that resists thrombogenesis and ultimately transforms into a neovessel capable of growth, remodeling, and repair [5]. The ideal small diameter TEVG for arterial bypass is readily available ("off-the-shelf"), resistant to thrombosis, aneurysmal dilatation and

* Corresponding author. Cardiovascular Tissue Engineering Program, Department of Cardiothoracic Surgery, The Heart Center, Nationwide Children's Hospital, 700 Children's Drive, T2294, Columbus, OH 43205, USA.
E-mail address: toshiharu.shinoka@nationwidechildrens.org (T. Shinoka).
[1] These authors equally contributed to this manuscript.

http://dx.doi.org/10.1016/j.atherosclerosis.2014.09.030
0021-9150/

ectopic calcification, easily implanted, biocompatible, and capable of transforming into neotissue comparable with that of native artery [6]. However, during the course of neovessel remodeling, these implants are susceptible to calcification, a potentially fatal long-term complication. The effect of scaffold physical structure on the development long-term calcific deposition in the neo-tissue of arterial TEVGs is currently unknown. The objective of this study was to characterize the calcification response between scaffolds fabricated from the same polymer but with different porosities by using a murine aortic implantation model in hopes of guiding future rational TEVG scaffold design.

2. Materials and methods

2.1. Animals

All animals received humane care in compliance with the National Institutes of Health (NIH) Guide for the Care and Use of Laboratory Animals. The Institutional Animal Care and Use Committee at Yale University approved the use of animals and all procedures described in this study. 8-week old female SCID/Bg mice were purchased from Jackson Laboratories (ME, USA).

2.2. Scaffolds

PLA–PLCL grafts were constructed using a dual cylinder chamber molding system from a nonwoven 100% poly(L-lactic acid) (PLA) fiber mesh (Biomedical Structures, RI, USA) and a 50:50 poly(L-lactic-co-ε-caprolactone) copolymer (PLCL) sealant (Gunze, Kyoto, Japan) as previously described [7]. PLA-nano grafts were composed of PLA nanofibers, which were constructed using electrospinning technology (Gunze). Total porosity, pore size, and fiber size of graft were measured via scanning electron microscopy.

2.3. Graft implantation

Twenty-eight PLA–PLCL grafts and twenty-five PLA-nano grafts were implanted as infra-renal aortic interposition conduits using standard microsurgical technique [8]. Animals were followed for 12 months following implantation to evaluate chronic calcification. Post-operatively, no drugs such as anti-platelet or anti-coagulant agents were used.

2.4. Histology, immunohistochemistry, and immunofluorescence

Explanted grafts at 4, 8, and 12 months after implantation, along with native abdominal aortas (control) were fixed in 4% paraformaldehyde and embedded in paraffin. 5 μm thick sections were then stained using standardized techniques for Alizarin Red S, Hematoxylin and Eosin (HE), Masson's Trichrome, and Elastica van Gieson (EVG). Quantitative analysis of calcific deposition was evaluated as a percentage of vessel cross-sectional area using Alizarin Red S staining, and measured by Image J software.

Endothelial cells (ECs), macrophages, vascular smooth muscle cells (VSMCs), and transcription factors of osteoblasts and osteoclasts were identified by immunohistochemical staining of paraffin-imbedded explant sections with rabbit anti-CD 31 (1:50, Abcam, MA, USA), rat anti-F4/80 (1:1000, AbD Serotec, Oxford, UK), mouse anti-smooth muscle actin (SMA, 1:500, DAKO, CA, USA), mouse anti-smooth muscle myosin heavy chain (SM-MHC, 1:400, Abcam), mouse anti-runt related transcription factor 2 (Runx2, 1:25, Abcam), and anti-receptor activator of nuclear factor kappa-B ligand (RANKL, 1:100, Abcam). Primary anti-bodies were detected using biotinylated goat anti-rat, -rabbit, and -mouse IgG (1:500, Vector, CA, USA) respectively, followed by binding of streptavidin–horseradish peroxidase and color development with 3,3-diaminobenzidine (Vector).

Immunofluorescent staining for SMA and SM-MHC as markers of SMCs was performed using mouse anti-SMA primary antibody (1:500, DAKO) and rabbit anti-SM-MHC primary antibody (1:1000, Abcam), and Alexa Fluor 647 anti-mouse IgG secondary antibody (1:300, Invitrogen, CA, USA) and Alexa Fluor 488 anti-rabbit IgG secondary antibody (1:300, Invitrogen), respectively. To evaluate expression of transcription factors of osteoblasts and osteoclasts, rabbit Runx2 primary antibody (1:500, Abcam) and

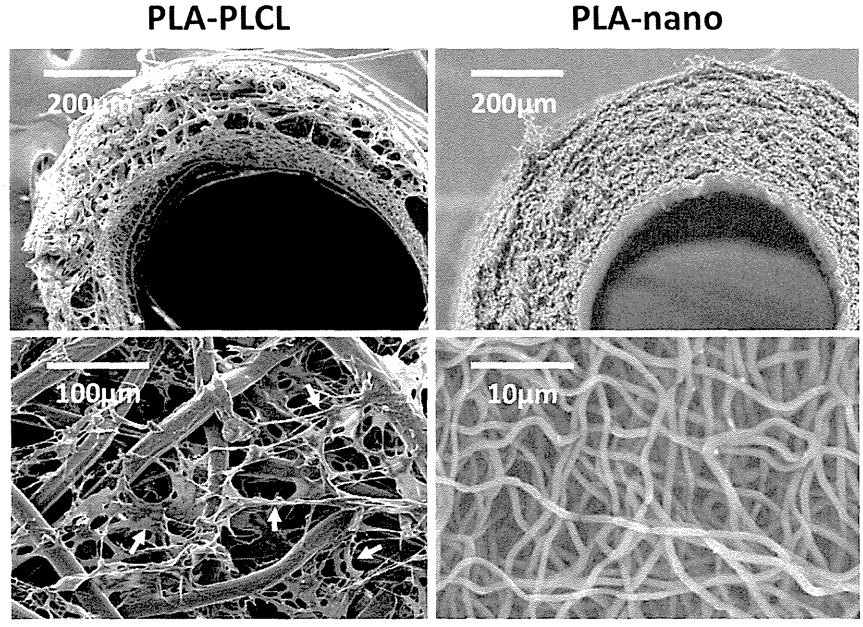

Fig. 1. Representative scanning electron microscopy images of implanted grafts. (Left) PLA–PLCL grafts were constructed from nonwoven 100% poly(L-lactic acid) (PLA) fiber mesh and a 50:50 copolymer sealant of poly(L-lactic-co-ε-caprolactone) (PLCL). Total porosity of PLA–PLCL was about 60%, and pore size was about 30 μm. Arrows indicate the PLCL sealant between PLA fibers. (Right) PLA-nano grafts were composed of PLA nanofibers, which were constructed using electrospinning technology. Total porosity of PLA-nano grafts was 70%, and pore size was about 5 μm. Inner luminal diameters of each graft were between 500 and 600 μm.

rabbit anti-RANKL primary antibody (1:100, Abcam), and Alexa Fluor 488 anti-rabbit IgG secondary antibody (1:300, Invitrogen) were used for immunofluorescent staining, respectively.

2.5. RNA extraction and reverse transcription quantitative polymerase chain reaction

Explanted grafts at 12 months after implantation and native abdominal aortas were frozen in optimal cutting temperature (OCT) compound (Sakura Finetek, CA, USA), and sectioned into twenty 30 μm sections using a Leica CM 1950 cryostat (Leica Biosystems, Wetzlar, Germany). Excess OCT compound was removed by centrifugation in PBS. Total RNA was extracted and purified using the RNeasy mini kit (Qiagen, CA, USA) according to the manufacturer's instructions. Reverse transcription was performed using High Capacity RNA-to-cDNA Kit (Applied Biosystems, CA, USA). All reagents and instrumentation for gene expression analysis were obtained from Applied Biosystems. Quantitative polymerase chain reaction (qPCR) was performed with a Step One Plus Real-Time PCR System using the TaqMan Universal PCR Master Mix Kit. Reference numbers for primers are: eNOS (Mm00435217_m1), Itgam (Mm0043455_m1), Runx2 (Mm00501580_m1), bone morphogenetic protein 2 (Bmp2, Mm01340178_m1), RANKL (Mm00441906_m1), and HPRT (Mm00446968_m1). The results were analyzed using the comparative threshold cycle method and normalized to endogenous reference gene HPRT, and reported results as relative values (ΔΔ CT) to the mean gene expression of control native aorta.

2.6. Statistical analysis

Results are expressed as mean ± standard deviation. The number of experiments is shown in each case. Data of continuous variables between PLA–PLCL group and PLA-nano group were evaluated by

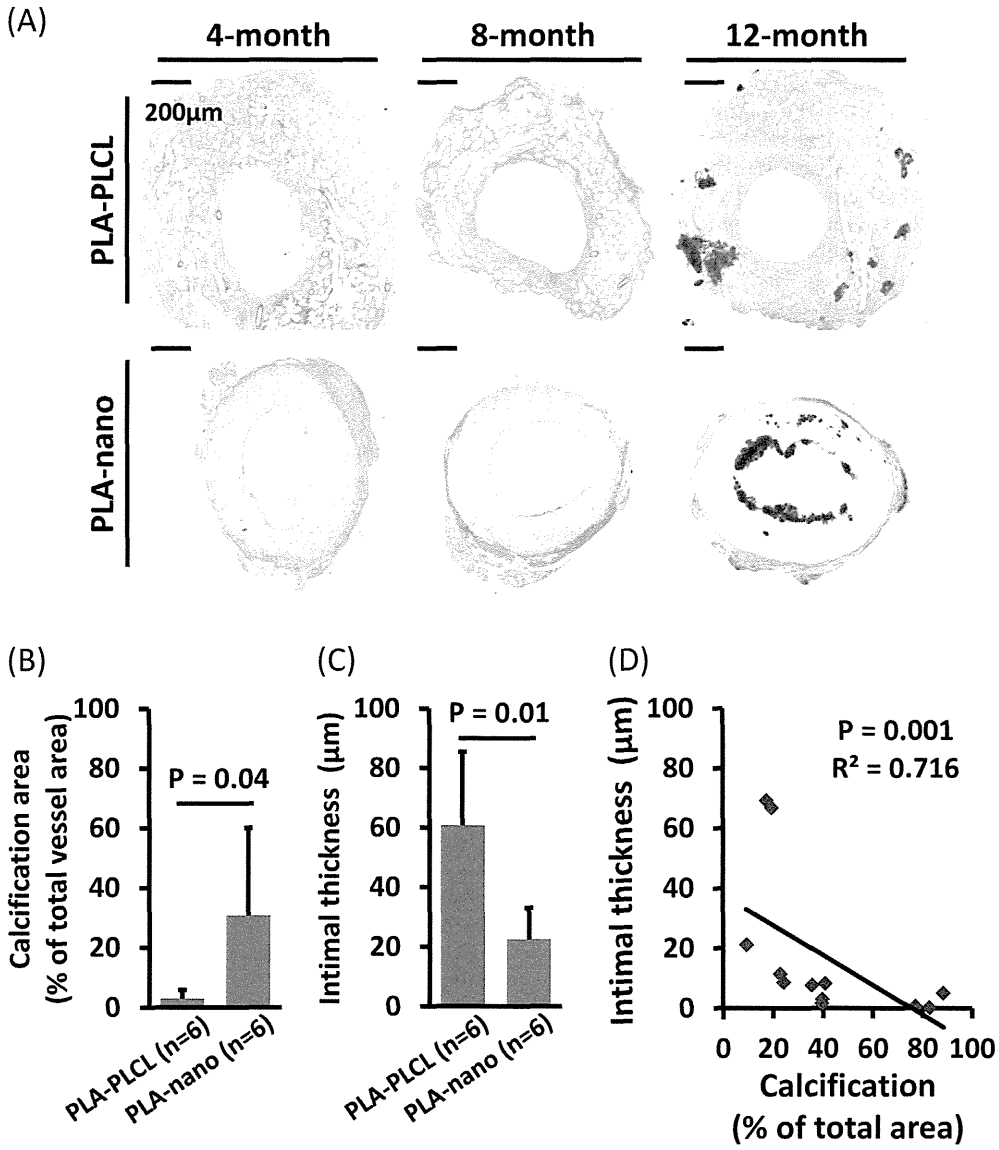

Fig. 2. Evaluation of calcified deposition and neointimal thickness. (A) Alizarin red S staining showed that neointimal calcified depositions were noted only in the PLA-nano grafts, although, positive staining the in the graft layer of both groups was observed 12 months after implantation. (B, C) Calcification area and intimal thickness were measured using Image J software (data presented as mean ± standard deviation), and evaluated by student's *t* test. Calcification area of the PLA-nano grafts were higher than that of PLA–PLCL grafts, and the neointima of PLA–PLCL grafts was thicker than that of PLA-nano grafts. (D) Spearman analysis was used to evaluate correlation between calcification area and intimal thickness, and there was negative correlation between these parameters.

student's *t*-test. Comparisons between multiple groups were done using one-way ANOVA followed by Tukey HSD. Spearman analysis was used for correlation analysis. A probability value of less than 0.05 was considered significant. All statistical analysis was performed using SPSS software (ver.20) (IBM, NY, USA).

3. Results

3.1. Graft construction

Total porosity of PLA–PLCL was about 60%, and average pore size was about 30 μm [7]. Diameter of PLA fiber of PLA–PLCL graft was about 20 μm. Total porosity of PLA-nano was about 70%, and average pore size was about 0.7 μm. Diameter of PLA-nano fiber was about 0.7 μm. Each scaffold was 3.0 mm in length and inner luminal diameters were between 500 and 600 μm (Fig. 1).

3.2. Animal survival

Twenty-eight PLA–PLCL grafts and twenty-five PLA-nano grafts were implanted as infra-renal interposition aortic conduits. Two animals in each group died during the peri-operative recovery period. PLA–PLCL grafts had dilated 4 months after implantation to have a luminal diameter of about 1.0 mm, which is almost twice as large as the implanted scaffold, however, these graft diameters stabilized at 1.0 mm for the remainder of the observation period. As a result of aneurysmal dilatation and subsequent graft rupture, twelve mice of the PLA–PLCL group died [9]. There was no aneurysmal formation and graft rupture in PLA-nano group, although 2 mice of the PLA-nano group died of undetermined causes during the course of observation period. Autopsy within 24 h after death did not identify any graft related complications such as rupture or occlusion.

3.3. Calcified depositions in neointimal layer and graft layer

Alizarin Red S staining of PLA-nano explants at 12 months demonstrated calcified depositions in the neointimal layer, which was defined as the layer between the endothelium and the graft material. Conversely, in the PLA–PLCL group, few grafts developed neointimal calcifications, although similar amounts of calcified depositions were present in the graft layer of both groups (Fig. 2A). Calcification area in all layers of PLA-nano was higher than that of PLA–PLCL (PLA-nano; 30.9 ± 29.1 vs PLA–PLCL; 3.0 ± 2.9, $p = 0.04$) (Fig. 2B). The neointima of the PLA–PLCL group was thicker than that of the PLA-nano group (PLA–PLCL; 60.7 ± 24.7 μm vs PLA-nano; 22.5 ± 10.5 μm, $p = 0.01$) (Fig. 2C), and there was negative correlation between calcification area (%) and intimal thickness ($y = -0.4965x + 37.597$, $r^2 = 0.716$, $p = 0.001$) (Fig. 2D).

3.4. PLA–PLCL supports well-organized neointimal formation with collagen and elastin

HE staining demonstrated complete degradation of PLCL sealant at 12 months following implantation, but some PLA fibers remained. There was dense cellular infiltration within PLA–PLCL grafts at the 12 month time point, and neotissue formation of PLA–PLCL graft resembled native aorta (Fig. 3). Extracellular matrix components including collagen and elastin were evaluated by Masson's Trichrome and EVG staining, and showed a positive deposition of both in the neointima of the PLA–PLCL group (Fig. 3). At 12 months, the PLA-nano group demonstrated abundant remaining fiber and a lack of cellular infiltration, yet there was a thin intimal layer on the luminal surface that was composed of collagen and elastin (Fig. 3).

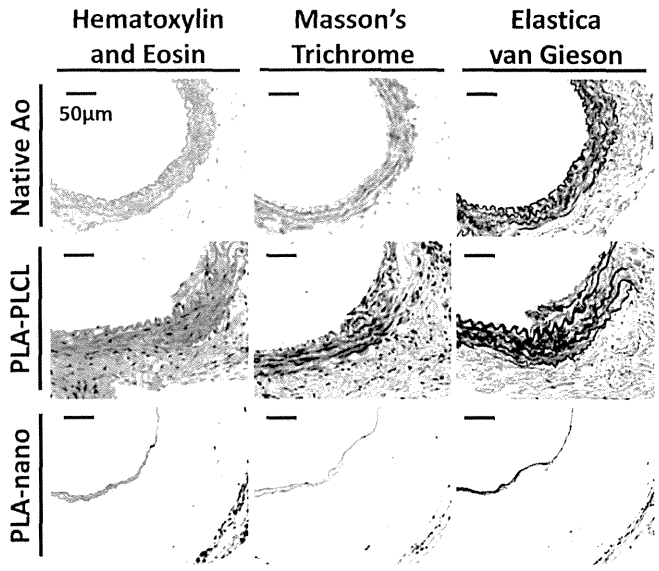

Fig. 3. Scaffold cellular infiltration and extracellular matrix deposition at 12 months after implantation. Hematoxylin and Eosin (HE) staining demonstrated dense cellular infiltration into PLA–PLCL graft and complete degradation of PLCL sealant. Masson's Trichrome and Elastica van Gieson (EVG) staining showed deposition of collagen and elastin in both the thick neointima of PLA–PLCL grafts and the thin neointima of PLA-nano grafts, respectively.

3.5. Endothelial cell coverage on luminal surface and macrophage infiltration into neotissue

Immunohistochemical staining for CD31 showed endothelial cell coverage of the luminal surface of both PLA–PLCL and PLA-nano at 12 months after implantation (Fig. 4A). Furthermore, there was no significant difference in gene expression of eNOS between two the groups (PLA–PLCL: 0.17 ± 0.06 vs PLA-nano: 0.20 ± 0.06, $p = 0.99$), although the levels of these were lower than that of native aorta (Fig. 4C).

F4/80 staining for macrophages showed that inflammation in the neotissue was present, however, there appeared to be regional differences between the localization of macrophages in the two groups (Fig. 4A). In the intimal layer, the density of macrophages in PLA-nano was higher than that of PLA–PLCL (F4/80 positive cells, PLA–PLCL; 68.1 ± 41.4/mm^2 vs PLA-nano; 188.3 ± 41.9/mm^2, $p = 0.007$) (Fig. 4B). In the scaffold layer, a higher density of macrophages was present around remaining PLA fibers in the PLA–PLCL group compared to the PLA-nano group (positive cells/mm^2, PLA–PLCL; 909.9 ± 143.4 vs PLA-nano; 105.6 ± 90.0, $p < 0.001$) (Fig. 4B). Relative gene expression of Itgam, a macrophage marker, tended to be higher in the PLA–PLCL group than in the PLA-nano group, reflecting increased cellular infiltration into the more porous PLA–PLCL scaffold, but there was no significant overall difference between the two groups (PLA–PLCL: 11.9 ± 4.0 vs PLA-nano: 6.8 ± 2.3, $p = 0.061$) (Fig. 4C).

3.6. Vascular smooth muscle cell proliferation in neointima of implanted grafts

Immunohistochemical staining for SMA and SM-MHC showed abundant VSMCs in the neointima of the PLA–PLCL group at 12 months after implantation (Fig. 5). On the other hand, there were few SMA or SM-MHC positive cells in the thin neointimal layer of the PLA-nano group (Fig. 5).